



HAL
open science

Method for High Frequency Underway N-2 Fixation Measurements: Flow-Through Incubation Acetylene Reduction Assays by Cavity Ring Down Laser Absorption Spectroscopy (FARACAS)

Nicolas Cassar, Weiyi Tang, Hans Gabathuler, Kuan Huang

► **To cite this version:**

Nicolas Cassar, Weiyi Tang, Hans Gabathuler, Kuan Huang. Method for High Frequency Underway N-2 Fixation Measurements: Flow-Through Incubation Acetylene Reduction Assays by Cavity Ring Down Laser Absorption Spectroscopy (FARACAS). *Analytical Chemistry*, 2018, 90 (4), pp.2839-2851. 10.1021/acs.analchem.7b04977 . hal-02619273

HAL Id: hal-02619273

<https://hal.science/hal-02619273>

Submitted on 25 May 2020

HAL is a multi-disciplinary open access archive for the deposit and dissemination of scientific research documents, whether they are published or not. The documents may come from teaching and research institutions in France or abroad, or from public or private research centers.

L'archive ouverte pluridisciplinaire **HAL**, est destinée au dépôt et à la diffusion de documents scientifiques de niveau recherche, publiés ou non, émanant des établissements d'enseignement et de recherche français ou étrangers, des laboratoires publics ou privés.

A method for high frequency underway N₂ fixation measurements: Flow-through incubation Acetylene Reduction Assays by Cavity ring down laser Absorption Spectroscopy (FARACAS)

Cassar Nicolas ^{1,2,*}, Tang Weiyi ¹, Gabathuler Hans, Huang Kuan ¹

¹ Division of Earth and Ocean Sciences, Nicholas School of the Environment, Duke University, Durham, NC 27708, USA

² Laboratoire des Sciences de l'Environnement Marin (LEMAR), UMR 6539 UBO/CNRS/IRD/IFREMER, Institut Universitaire Européen de la Mer (IUEM), Brest, France.

* Corresponding author : Nicolas Cassar, email address : nicolas.cassar@duke.edu

Abstract :

Because of the difficulty in resolving the large variability of N₂ fixation with current methods which rely on discrete sampling, the development of new methods for high resolution measurements is highly desirable. We present a new method for high-frequency measurements of aquatic N₂ fixation by continuous flow-through incubations and spectral monitoring of the acetylene (C₂H₂, a substrate analog for N₂) reduction to ethylene (C₂H₄). In this method, named "Flow-through incubation Acetylene Reduction Assays by Cavity ring-down laser Absorption Spectroscopy" (FARACAS), dissolved C₂H₂ is continuously admixed with seawater upstream of a continuous-flow stirred-tank reactor (CFSTR) in which C₂H₂ reduction takes place. Downstream of the flow-through incubator, the C₂H₄ gas is stripped using a bubble column contactor and circulated with a diaphragm pump into a wavelength-scanned Cavity Ring Down laser absorption Spectrometer (CRDS). Our method provides high-resolution and precise mapping of aquatic N₂ fixation, its diel cycle, and its response to environmental gradients, and can be adapted to measure other biological processes. The short-duration of the flow-through incubations without pre-concentration of cells minimizes potential artefacts such as bottle containment effects while providing near real-time estimates for adaptive sampling. We expect that our new method will improve the characterization of the biogeography and kinetics of aquatic N₂ fixation rates.

II. INTRODUCTION

The net inventory of organic nitrogen is in great part controlled by microbially-mediated redox pathways, including dinitrogen (N_2) fixation, the reduction of N_2 to ammonium. This biological process, catalyzed by the enzyme nitrogenase in select autotrophic and heterotrophic prokaryotes¹⁻², influences terrestrial and oceanic fertility and, in the process, the global carbon cycle³⁻⁶. In the marine environment, N_2 fixation is regulated by a wide variety of environmental factors, including light level, temperature, elemental stoichiometry and trace metal availability⁷⁻¹⁶. The combined effect of these and other yet-to-be-identified factors leads to large spatial heterogeneity in marine N_2 fixation. In fact, the episodicity and patchiness of N_2 fixation, which cannot be captured with current methodologies which rely on discrete sampling^{5, 17-19}, have been hypothesized to contribute to the large disparity between incubation-based and geochemical-tracer estimates of oceanic N_2 fixation budgets^{5, 20-21}. The limited number of discrete observations have also made it difficult to decipher controls on N_2 fixation rates²². New analytical techniques that provide sensitive and high resolution assessments of N_2 fixation rates are therefore needed to better characterize the biogeography of N_2 fixation and close the global N budget. To that end, we present a new ship-based method for high-frequency underway estimates of N_2 fixation. To the best of our knowledge, our method is the first to allow underway near real-time estimates of N_2 fixation rates. It can be used to elucidate the biogeography of aquatic N_2 fixation, with the overarching goal of improving our understanding of the nitrogen budget and its physical and biogeochemical forcings.

III. MATERIALS AND METHODS

Description of the Flow-through incubations Acetylene Reduction Assays by Cavity ring-down laser Absorption Spectroscopy (FARACAS)

Overview of the FARACAS method

N₂ fixation rates are commonly derived from Acetylene Reduction Assays (ARAs)²³⁻²⁴. Building on a method developed by our laboratory for the study of N₂ fixation in terrestrial environments²⁵, our new method, “Flow-through incubation Acetylene Reduction Assays by Cavity ring-down laser Absorption Spectroscopy” (FARACAS) consists of 4 modules (Fig. 1): 1) a dual channel peristaltic pump for precise and continuous admixing of high-purity dissolved acetylene (C₂H₂) with seawater, 2) a constant-volume continuous flow stirred tank reactor (CSTR) for the flow-through incubation where the C₂H₂ reduction to ethylene (C₂H₄) takes place, 3) a bubble column multiphase reactor for the C₂H₄ gas stripping, and 4) continuous measurements of the flow-through C₂H₄ by wavelength-scanned Cavity Ring-Down laser Absorption Spectroscopy (CRDS, Picarro, CA). The fixation rates are normalized to water volume or chlorophyll concentrations by measuring chlorophyll simultaneously and continuously with an underway fluorometer. Below we describe each module in detail. Pictures of various components of the FARACAS method are also presented in Fig. S1.

Upstream of the flow-through incubation

Prior to the flow-through incubation chamber, a custom-built trace-metal clean towfish with an air-operated double diaphragm pump (Wilden, CA) is used to gently and continuously bring the seawater to the laboratory²⁶. Such a sampling approach has been used for incubations in the past²⁷⁻²⁸. We further confirmed during our field trials that sampling was not disruptive to the diazo-

1
2
3 trophic community by comparing our results to $^{15}\text{N}_2$ incubations on samples collected inde-
4 pendently with Niskin bottles (see discussion below).
5
6

7
8 The C_2H_2 is prepared by reacting high-purity calcium carbide (CaC_2 , Acros Organics) with de-
9 ionized water in a Tedlar bag according to the reaction $\text{CaC}_2 + 2 \text{H}_2\text{O} \rightarrow \text{C}_2\text{H}_2 + \text{Ca}(\text{OH})_2$. Pre-
10 paring the C_2H_2 from CaC_2 on site is simpler than transporting acetylene cylinders, and most
11 importantly, provides C_2H_2 with less C_2H_4 impurities than what is currently commercially avail-
12 able. High-purity (prepurified) C_2H_2 cylinders have significant levels of C_2H_4 contaminant, usu-
13 ally ranging from 5 to 12 ppm in a 10% (v/v) C_2H_2 incubation depending on cylinder discharge.
14 By comparison, C_2H_2 produced from calcium-carbide contains around 1.5 ppm C_2H_4 per 10% of
15 C_2H_2 , and 400 ppb after dissolution in seawater. We are exploring other options for further re-
16 ducing the C_2H_4 impurities.
17
18
19
20
21
22
23
24
25
26
27

28
29 We dissolve the C_2H_2 gas in 0.2 μm -filtered seawater to a final saturation of 70% (v/v %), and
30 continuously admix 15 ml min^{-1} of this solution (Q_{tracer}) to a stream of 85 ml min^{-1} of unfiltered
31 seawater from the towfish (Q_{sw}) using a dual-channel peristaltic pump (Masterflex) at a ratio of
32 approximately 1/6 for a final C_2H_2 concentration c.10%. The inner diameters of the seawater
33 and tracer tubings are 4.8 and 1.6 mm, respectively. A correction for the dilution of the seawater
34 with the C_2H_2 -filtered seawater solution is applied to our final estimates of acetylene reduction
35 rates. Addition of the C_2H_2 in a dissolved form has several advantages: 1) it further reduces the
36 C_2H_4 impurities because of the low solubility of C_2H_4 relative to C_2H_2 (Fig. 2), 2) it limits the
37 risk of not reaching full C_2H_2 gas-liquid equilibration, and compared to mixing and shaking of
38 gaseous C_2H_2 , as performed using the traditional approach, 3) it is more precise, and 4) less per-
39 turbing to the microbial cells.
40
41
42
43
44
45
46
47
48
49
50
51
52
53

54
55 ***Flow-through incubation with a continuous flow stirred tank bioreactor***
56
57
58
59
60

1
2
3 The 10% C₂H₂-amended seawater is pumped into a modified 9 liter flow-through incubation
4 reactor (Chemglass, NJ) at a rate of 100 ml min⁻¹ (Fig. 1a). The glass chemostat-style reaction
5 vessel is thermoregulated to ambient seawater temperature with a water-jacket and gently stirred
6 with a crossed magnetic stirrer at the bottom of the vessel. The flow-through incubator is kept in
7 a dark enclosure to avoid contamination from ambient light. Light in the enclosure is provided by
8 a bank of LED lights with their intensity computer-controlled (LabVIEW) to vary as a function
9 of local time of day and geographical coordinates. Neutral blue density filters (Pale Blue, E-
10 Color) are used to emulate light quality at the ocean surface. To limit biofouling, the incubation
11 chamber is acid-cleaned nightly or every other night when N₂ fixation rates are generally low.
12 Variations in the background C₂H₄ (i.e. contaminant in C₂H₂ and naturally occurring in seawater)
13 are accounted for by bypassing the flow-through incubation chamber every few hours for 30
14 minutes at predetermined computer-controlled (LabVIEW) intervals using a liquid-inlet VICI
15 Valco valve. The C₂H₄ signal right after bypasses is biased high because of the longer incubation
16 time during the bypass. This biased signal, which is most pronounced when N₂ fixation rates are
17 high, should be corrected or omitted from the final N₂ fixation estimates. In future applications,
18 we will lower the frequency of bypasses to limit the instances of change in incubation duration
19 associated with these bypasses. We have found that the bypass C₂H₄ signals are stable with little
20 drift over time (see field deployment section below).

21 22 23 24 25 26 27 28 29 30 31 32 33 34 35 36 37 38 39 40 41 42 43 44 45 ***Ethylene stripping with a bubble column contactor***

46
47
48 Downstream of the incubation chamber, a custom-built bubble column contactor is used to ex-
49 tract the dissolved C₂H₄ through sparging. Similar designs are often used in gas-liquid reactions
50 under continuous flow and turbulent conditions to promote rapid exchange of gases²⁹⁻³⁰. At the
51 base of the cylindrical column, a stream of uniform low-volume bubbles is used to strip the C₂H₄
52
53
54
55
56
57
58
59
60

1
2
3 out of the seawater. The bubbles are produced by flowing 35 ml min^{-1} of C_2H_4 -free air, provided
4
5 by a pump or a gas tank and regulated with a mass flow controller (OMEGA), through a medium
6
7 porosity glass-frit sparger (Chemglass, NJ). The homogenous bubbly flow regime at the base
8
9 evolves into a heterogeneous slug or churn-turbulent flow regime as the small bubbles coalesce
10
11 into larger bubbles along the flow path. The gas stream exits from the top of the bubble column
12
13 contactor and into the CRDS in flow-through mode while the flowing seawater outflows from a
14
15 side arm of adjustable height. To limit the risk of flooding the CRDS, the water level in the bub-
16
17 ble column contactor is continuously monitored with frequency modulator sensors which are
18
19 corrected with a temperature sensor, and recorded in LabVIEW. A set of warning LED lights
20
21 illuminating the column change color as a function of water height to alert the operator should
22
23 the water level rise too high. As a final safety, a threshold contactor at the top of the column
24
25 made of dental stainless steel wire uses conductance as a trigger mechanism operating two valves
26
27 upstream of the CRDS. Should water reach this critical level, the valves isolate the CRDS there-
28
29 by preventing water from entering the optical cavity and damaging the instrument.
30
31
32
33
34
35

36 ***Ethylene measurements by Cavity Ring-Down laser absorption Spectroscopy (CRDS)***

37
38

39 In ARA, C_2H_4 production is conventionally measured by gas chromatography with flame ioniza-
40
41 tion detection (GC-FID). The use of CRDS to monitor C_2H_4 production kinetics in ARA was
42
43 first described by Cassar et al.²⁵. The main advantages of the CRDS approach are up to three
44
45 orders of magnitude greater sensitivity than GC-FID and real-time monitoring of the acetylene
46
47 reduction. The new method has been used to study environmental forcings and short-term kinet-
48
49 ics of terrestrial N_2 fixation in the soil bacterium *Azotobacter vinelandii*, in mosses and lichens
50
51 from contrasting ecosystems, and to identify a formerly unknown true moss-diazotrophic cyano-
52
53 bacteria association in a widespread moss species^{25,31}. As opposed to the GC-FID approach, the
54
55
56
57
58
59
60

1
2
3 spectral detection of C₂H₄ in a CRDS is non-destructive. The C₂H₄ concentration is estimated
4
5 based on the measurements of the decay rate of a laser light pulse sent into an optical cavity con-
6
7 sisting of high reflectivity mirrors which provides enhanced effective absorption path length. For
8
9 the FARACAS method, we use a Picarro CRDS C₂H₄ analyzer (model G1106, Santa Clara, CA,
10
11 USA). For our purposes, this analyzer offers several key benefits, including: 1) continuous real-
12
13 time C₂H₄ measurements with high linearity over a wide dynamic range from ppb to ppm with
14
15 high sensitivity and precision (according to manufacturer's specs, 2 and 0.2 ppbv (3 σ) over 5
16
17 and 300 seconds, respectively), 2) fast response time and high frequency measurements (se-
18
19 seconds), 3) low drift (according to manufacturer's specs, \pm 4 and 10 ppbv over 24 hours and 1
20
21 month, respectively), 4) high chemical specificity with negligible interferences from C₂H₂, CO₂,
22
23 methane and water, and 5) stable readings under varying conditions of temperature, humidity and
24
25 vibrations. Further description of the instrument's application to ARA is provided in Cassar et al.
26
27
28
29
30
31 .
32

33 ***Additional hardware and software***

34
35
36
37 Additional hardware and a program developed in LabVIEW are used to monitor, control, dis-
38
39 play, and record various aspects of the FARACAS system (Fig. 1b). More specifically, the in-
40
41 struments and software are used to: 1) manually actuate the Valco valve, or select and configure
42
43 valve recipes (frequency and duration of the automated bypasses of the flow-through incubation
44
45 chamber), 2) automatically adjust the LED light intensity in the flow-through incubator based on
46
47 the sun elevation and intensity, calculated based on local time and geographical coordinates as
48
49 provided by a GPS receiver. Sun path, including azimuth, sunrise and sunset, and various defini-
50
51 tions of twilights are also calculated. Several properties are monitored, displayed and recorded
52
53 for diagnostic purposes, including 1) ambient room temperature, humidity and atmospheric pres-
54
55
56
57
58
59
60

1
2
3 sure, 2) seawater temperature at the inlet, in the flow-through incubation chamber, in the bubble
4 column contactor, and from the outflow to detect anomalous changes in temperature in the incu-
5 bation chamber and the rest of the seawater lines, 3) stripping gas and seawater flow rates, and
6 water level in the bubble column contactor to assess how changes in these properties may affect
7 the C_2H_4 extraction efficiency (see theoretical considerations below), 4) actual light intensity in
8 the flow-through incubator, light on/off status, and the light setpoint according to the sun path,
9 and 5) valve position. Many of these properties are displayed as a function of time for the last 24
10 hrs, including the C_2H_4 concentration and light intensity for real-time diagnostics and observa-
11 tions such as onboard detection of the diel cycle in N_2 fixation rates. In the same interface, the
12 cruise track is overlaid on a map which shows user-selected properties, such as satellite images
13 of chlorophyll, sea surface temperature, or sea surface height (see Fig. S2 as an example). A pan-
14 el with annunciator lights at the bottom of the user interface indicates the status of operation
15 (green when running smoothly, orange for warning/caution, red for error) for 1) the water level
16 in the bubble column contactor, 2) number of GPS satellites within reach, 3) valve position and
17 time remaining at current position, 4) status of the microcontroller and CRDS, 4) sun elevation
18 (% light intensity), and 5) proper saving of the file. The software also issues error codes should
19 the water level in the bubble column contactor trigger the shutoff valves. As part of the software,
20 an event log is also used as a digital lab logbook. A second software is used for *a posteriori* data
21 evaluation and visualization, including zooming, and time-averaging and integrating functions.
22
23
24
25
26
27
28
29
30
31
32
33
34
35
36
37
38
39
40
41
42
43
44
45
46

47 **IV. RESULTS AND DISCUSSION**

48 **Impetus for new methods**

49 *Importance of N_2 fixation and paucity of measurements in the oceans*

1
2
3 The export of organic carbon from the surface to deep waters is dependent on the supply of new
4 nutrients to the euphotic zone. As one of the main macronutrients limiting primary production in
5 the oceans, nitrogen has a tremendous impact on marine ecosystems and the global carbon cycle
6
7
8
9
10³²⁻³⁴. In the last two decades, it has become increasingly evident that the microbially-catalysed
11 reduction of atmospheric N₂ to ammonium is an important, but difficult to quantify, source of
12 exogenous N in the oligotrophic waters of the tropics and subtropics comprehensive review in³⁵.
13
14
15 In these regions, N₂ fixation is believed to be a significant contributor to net carbon export^{5, 17, 34,}
16
17
18³⁶⁻⁴⁰. Cyanobacterial diazotrophs, such as the nonheterocystous filamentous genus *Trichodes-*
19
20
21
22
23
24
25
26
27
28
29
30
31
32
33
34
35
36
37
38
39
40
41
42
43
44
45
46
47
48
49
50
51
52
53
54
55
56
57
58
59
60

Based on a variety of independent estimates, including scaling of field observations, biogeochemical models and geochemical tracers, the global marine N₂ fixation flux is estimated to be in the range of 53-200 Tg N yr⁻¹, representing approximately half of the new nitrogen to the oceans^{19, 33, 48, 50-56}. Mahaffey et al.⁵ hypothesized that discrete observations are missing substantial N₂ fixation events or regions based on the discrepancy relative to the geochemical approaches. More recently, Somes et al.²⁰ used nitrogen isotope observations and a marine biogeochemical model to argue that previous studies significantly underestimate oceanic N₂ fixation. The large uncertainty in N₂ fixation estimates is partly attributable to the paucity of measurements and our rela-

tively limited understanding of the factors regulating N₂ fixation^{17,57}. There is, thus, broad scientific interest in a method, such as FARACAS, for surveying of the high spatiotemporal variability in oceanic N₂ fixation rates at higher resolution.

Current methods for measuring N₂ fixation rates

Since the first reports of the competitive inhibition of N₂ fixation by triple-bonded C₂H₂^{23,58-61}, the reduction of C₂H₂ to C₂H₄ in ARA has been one of the most common methods for estimating nitrogenase activity²³⁻²⁴. N₂ fixation is for all intents and purposes quantitatively inhibited under saturating C₂H₂. Although ARA has some limitations⁶²⁻⁶⁴, the approach provides a simple and inexpensive way to estimate N₂ fixation. C₂H₄ production in ARA is generally measured by GC-FID, but innovative methods with higher sensitivity have also been developed for discrete observations⁶⁵⁻⁶⁸. C₂H₂ reduction rates ultimately needs to be converted to N₂ fixation rates. Whereas the net biological reduction of N₂ to NH₃ requires six⁶⁹ to eight electrons (additional 2 electrons for H₂ production)⁷⁰⁻⁷¹, C₂H₂ reduction to C₂H₄ by nitrogenase requires only two electrons: $C_2H_2 + 2e^- + 2H^+ \rightarrow C_2H_4$. Hence, based on this stoichiometry and depending on the hydrogenase activity of the nitrogenase enzyme, the biological reduction of N₂ is predicted to be one third to one fourth of the ARA measurements. Because the various isotopes of N have similar kinetic properties, ¹⁵N₂ tracer incubations provide a benchmark against which other methods such as ARAs are generally calibrated. The two methods generally show good agreement, albeit with some discrepancies, which may in part be attributed to: 1) C₂H₂/N₂ conversion factors deviating from theoretical predictions^{63,67,72-73}, 2) the methods assessing different rates (i.e., net vs. gross N₂ fixation)⁷⁴ and underestimation of N₂ fixation when not accounting for ¹⁵N in the dissolved organic pool⁷⁵⁻⁷⁶, and 3) other experimental and analytical artefacts associated with both methods, including below saturation levels of C₂H₂⁶⁷, C₂H₂ modifications of the metabolic activ-

ities of the diazotrophic and microbial communities ^{64, 77}, incomplete equilibration of the ¹⁵N with the incubated seawater ⁷⁸, and contamination of commercial ¹⁵N₂ gas tanks ⁷⁹.

Theoretical considerations and N₂ fixation calculations with the FARACAS method

Steady-state conditions

To illustrate the approach, we first assume steady-state for simplicity. Abbreviations used in this study are summarized in Table 1. With a flow-through incubation chamber with homogeneous mixing and no headspace, the C₂H₄ concentration at the outlet of the chamber ($[C_2H_4]_{total}$) is a function of the C₂H₄ contaminant from the calcium-carbide produced C₂H₂, the C₂H₄ naturally present in seawater, and the C₂H₄ produced in the reaction chamber through diazotrophic C₂H₂ reduction. We combine the first two terms into a time-variable tracer offset of b . $[C_2H_4]_{total}$ is therefore equal to the sum of $[C_2H_4]$ due to C₂H₂ reduction in the reaction chamber ($[C_2H_4]_{ARA}$) and the tracer b . Assuming perfect mixing and constant diazotrophic acetylene reduction rates, $[C_2H_4]_{ARA}$, the term of interest, is a function of the volumetric C₂H₂ reduction rate (N_{fixAR}) (in ppb C₂H₄ min⁻¹) multiplied by the residence time in the incubation chamber (τ , equivalent to the “space time” or “hydraulic retention time” in our case of a constant-density reactor), where τ is equal to the volume of the incubation chamber (V) divided by the seawater flow rate (Q_{total}):

$$[C_2H_4]_{ARA} = N_{fixAR} \frac{V}{Q_{total}} \quad (1)$$

where N_{fixAR} is equal to the volumetric N₂ fixation rate (N_{fix}) times a C₂H₂/N₂ conversion factor.

By mass balance, the amount of C₂H₄ in the stripping gas must be equal to the amount entering

the bubble column contactor times an extraction efficiency factor $X = \frac{Q_{strip}[C_2H_4]_{strip}}{Q_{total}[C_2H_4]_{total}}$, where X

varies from 0 to 1 and $[C_2H_4]_{strip}$, Q_{strip} and Q_{total} refer to ethylene concentration in the strip

1
2
3 gas exiting the bubble column contactor, and the gas and water flow rates, respectively. It fol-
4
5 lows that $[C_2H_4]_{strip}$ can be expressed as:

$$[C_2H_4]_{strip} = X \frac{Q_{total}}{Q_{strip}} \left(N_{fixAR} \frac{V}{Q_{total}} + b \right) \quad (2)$$

6
7
8
9
10
11
12 Below, we describe the kinetics of the C_2H_4 signal in the bubble column contactor and in the
13
14 flow-through incubation chamber, and present a derivation of the calculations of N_2 fixation rates
15
16 based on the FARACAS method.
17
18

19 20 ***Transient conditions***

21 22 *Kinetics in the Bubble column contactor*

23
24
25 The interdependent factors influencing the mass transfer efficiency in bubble column reactors
26
27 have been extensively studied see reviews by ^{80, 81} and will therefore only be briefly described.
28
29 However, our approach differs from most industrial applications in that our objective is not to
30
31 optimize mass transfer but the concentration of C_2H_4 in the stripping gas, with the corollary that
32
33 the stripping gas flow rate is lower than the liquid flow rate under our configuration. The total
34
35 volume of the bubble column contactor (V_{bc}) is the sum of the volumes of the liquid (V_l), head-
36
37 space (V_{hs}), and bubbles (V_{bb}), with V_{lbb} reflecting the dispersion mixture of liquid and bubbles.
38
39 The time-derivative of the concentration of ethylene in the stripping gas phase (i.e. bubbles and
40
41 the headspace volumes of the column) is a function of gas exchange with the liquid phase and
42
43 fluxes in and out of the bubble column contactor:
44
45
46
47
48
49
50
51
52
53
54
55
56
57
58
59
60

$$\begin{aligned}
 (V_{lbb}(\varepsilon_g) + V_{hs}) \frac{d[C_2H_4]_{strip}}{dt} \\
 = k_L a V_{lbb} (1 - \varepsilon_g) ([C_2H_4]_{total} - \alpha [C_2H_4]_{strip}) \\
 - Q_{strip} [C_2H_4]_{strip} + Q_{strip} [C_2H_4]_o
 \end{aligned} \tag{3}$$

where $[C_2H_4]_o$, k_L , ε_g , a and α are the ethylene concentration in the gas used as a strip gas prior to the column, the liquid phase mass transfer coefficient (m min^{-1}), the gas holdup (the ratio of gas phase volume to total volume of the dispersion), the contactor's effective specific gas-liquid interfacial area (i.e. interfacial area per unit volume of dispersion, $\text{m}^2 \text{m}^{-3}$), and the dimensionless Ostwald solubility coefficient, respectively. We use k_L under the assumption that the resistance to mass transfer in the gaseous phase is negligible compared to that in the aqueous phase⁸⁰⁻⁸¹. Factors influencing the mass transfer coefficient, such as gas-liquid contact time, hydrodynamics, bubble size distribution, and gas pressure are often interdependent. For example, the contactor's effective specific gas-liquid interfacial area is a function of the gas holdup and the sauter mean bubble diameter (d_s) according to the equation $a = \frac{6\varepsilon_g}{d_s}$. The extraction efficiency is thus predicted to increase with the relative proportion of the gas phase and inversely to bubble size. Previous studies have shown that the gas holdup and mass transfer improve with superficial gas velocity and decreasing column diameter⁸². We tried to maximize these terms with narrow tubing and column, and high surface area-to-volume bubbles and sparging gas flow rate. In the latter case, a compromise between extraction efficiency and dilution of the signal measured on the CRDS must be taken into account (see equations and empirical results below). Temperature, salinity, and surfactants may also affect the extraction efficiency through their effect on the molecular diffusivity, gas solubility, gas holdup, the viscosity of the water, and bubble characteristics and breakup and coalescence⁸³⁻⁸⁶. C_2H_4 solubility increases with decreasing temperature and

1
2
3 salinity (Fig. 2)⁸⁷⁻⁸⁸. Salinity affects C₂H₄ solubility through the salting-out effect, but in open
4 ocean settings (generally < ± 3 PSU), the effect will be small and within the error of our meas-
5 urements. In regions with high variability in these properties, corrections for changes in the C₂H₄
6 transfer coefficient should be applied, or accounted for with more frequent bypass calibrations.
7

8
9
10 We neglect the last term on the right-hand side of Eq. (3) because [C₂H₄]_o is negligible prior to
11 entering the column. The solution to the first-order linear differential Eq. (3) is:
12

$$13 \quad [C_2H_4]_{strip} = [C_2H_4]_{strip_o} e^{-\frac{(\alpha k_L a V_{lbb}(1-\varepsilon_g) + Q_{strip})_t}{(V_{lbb}(\varepsilon_g) + V_{hs})}} + \frac{k_L a V_{lbb}(1-\varepsilon_g)}{\alpha k_L a V_{lbb}(1-\varepsilon_g) + Q_{strip}} (1$$

$$14 \quad - e^{-\frac{(\alpha k_L a V_{lbb}(1-\varepsilon_g) + Q_{strip})_t}{(V_{lbb}(\varepsilon_g) + V_{hs})}}) [C_2H_4]_{total} \quad (4)$$

15
16
17 See supporting information for the full derivation. The first term on the right-hand side of Eq. (4)
18 illustrates that the transient ethylene concentration in the strip gas at any time (t) is a function of
19 the ethylene concentration at some previous time (t₀) multiplied by a relaxation rate which is a
20 function of the e-folding residence time of the ethylene in the bubbles and headspace volumes.
21
22 The second term in Eq. (4) shows that the ethylene concentration in the strip gas at any time (t) is
23 also a function of the net exchange of ethylene between the liquid and gas phases. In order to
24 explore the factors influencing the mass transfer efficiency, we assume that steady-state is
25 achieved with a constant N₂ fixation rate in the flow-through incubation chamber upstream of the
26 bubble column contactor (i.e. t → ∞ and [C₂H₄]_{total} is assumed to be constant):
27
28
29
30
31
32
33
34
35
36
37
38
39
40
41
42
43
44
45
46
47

$$48 \quad \frac{[C_2H_4]_{strip}}{[C_2H_4]_{total}} = \frac{k_L a V_{lbb}(1-\varepsilon_g)}{\alpha k_L a V_{lbb}(1-\varepsilon_g) + Q_{strip}} \quad (5)$$

49
50
51
52
53 Eq. (5) shows that at steady-state, the ratio of concentrations of ethylene in the strip and liquid
54 phases is a function of the relative exchanges between the liquid and gas phase. When the trans-
55
56
57
58
59
60

fer from the liquid to gas phase is fast compared to the stripping gas flow rate ($\alpha k_L a V_{lbb}(1 - \varepsilon_g) \gg Q_{strip}$), the $[C_2H_4]_{strip}$ should be equal to the one in the liquid phase accounting for the dimensionless Ostwald solubility constant. Conversely, when the stripping gas flow rate is much larger than the gas exchange kinetics between the liquid and gas phases ($Q_{strip} \gg \alpha k_L a V_{lbb}(1 - \varepsilon_g)$), the concentration of ethylene in the stripping gas asymptotes to zero because of dilution. In other words, although the bubble column contactor can theoretically reach an extraction efficiency of 100%, the highest concentration of ethylene achievable in the stripping gas is dictated by its solubility. This may in part explain our extraction efficiency of around 66% (see below), with the dimensionless Ostwald solubility coefficient predicting an upper bound of approximately 90% of the ethylene in the stripping gas at equilibrium under ambient conditions (Fig. 2b). We multiply both sides of Eq. (5) by $\left(\frac{Q_{strip}}{Q_{total}}\right)$ to calculate the extraction efficiency:

$$\begin{aligned}
 X &= \frac{Q_{strip}[C_2H_4]_{strip}}{Q_{total}[C_2H_4]_{total}} = \left(\frac{Q_{strip}}{Q_{total}}\right) \left(\frac{k_L a V_{lbb}(1 - \varepsilon_g)}{\alpha k_L a V_{lbb}(1 - \varepsilon_g) + Q_{strip}}\right) \\
 &= \left(\frac{1}{Q_{total}}\right) \left(\frac{k_L a V_{lbb}(1 - \varepsilon_g)}{\left(\frac{1}{Q_{strip}} \alpha k_L a V_{lbb}(1 - \varepsilon_g) + 1\right)}\right)
 \end{aligned} \tag{6}$$

The extraction efficiency is therefore predicted to decline as Q_{total} increases. As Q_{strip} increases, the extraction efficiency rises plateauing at $X = \left(\frac{k_L a V_{lbb}(1 - \varepsilon_g)}{Q_{total}}\right)$. The extraction efficiency is also maximized ($X = 1$) with a ratio of water to stripping gas flow rates which keeps up with the ratio of kinetics of liquid-to-gas transfer vs. kinetics of gas-liquid and gas exiting the column contactor headspace (i.e. $\left(\frac{Q_{total}}{Q_{strip}}\right) = \left(\frac{k_L a V_{lbb}(1 - \varepsilon_g)}{\alpha k_L a V_{lbb}(1 - \varepsilon_g) + Q_{strip}}\right)$). Otherwise, a fraction of the ethylene exits the bubble column in the dissolved form. Based on Eq. (5), one ultimately needs to

decrease Q_{strip} to the extent possible while maximizing the mass transfer efficiency to optimize $[C_2H_4]_{strip}$ and improve the detection limit.

Kinetics in the flow-through incubation chamber

In the discussion above on the kinetics in the bubble column contactor, we assumed for simplicity a constant dissolved C_2H_4 concentration. Below, we describe the kinetics of the transient ethylene concentration in the flow-through incubation chamber and for the FARACAS method overall. By mass balance, the time-derivative of the concentration of C_2H_4 in the flow-through incubation chamber ($[C_2H_4]_{chamber}$) is a function of the influx of ethylene contaminant in the chamber (b), diazotrophic acetylene reduction in the chamber (N_{fixAR}), and efflux of C_2H_4 from the chamber:

$$\frac{d[C_2H_4]_{chamber}}{dt} = \frac{b * Q_{total}}{V} + N_{fixAR} - \frac{[C_2H_4]_{chamber} * Q_{total}}{V} \quad (7)$$

Solving the differential equation and rearranging, we find that the acetylene reduction rate in the incubation chamber can be calculated from consecutive C_2H_4 measurements over a period Δt ($\Delta t = t - t_0$) according to the following equation:

$$N_{fixAR} = \frac{Q_{total}}{V} \left(\frac{[C_2H_4]_{chamber} - [C_2H_4]_{chamber_0} e^{-\frac{Q_{total}\Delta t}{V}}}{1 - e^{-\frac{Q_{total}\Delta t}{V}}} - b \right) \quad (8)$$

A full derivation of this analytical solution is presented in the supporting information. At steady-state (i.e. $t \rightarrow \infty$), $[C_2H_4]_{chamber} = \frac{N_{fixAR} * V}{Q_{total}} + b$, which is identical to equation (1) when accounting for the background tracer C_2H_4 concentration.

In order to calculate the C_2H_4 in the stripping gas which is measured by the CRDS (i. e. $[C_2H_4]_{strip}$), one therefore needs to account for the kinetics in the flow-through chamber and in the bubble column contact as described in the sections above. In the current configuration, the e-folding response time of the bubble column contactor is approximately 2-3% of the one of the flow-through incubation chamber. In this respect, the response kinetics of the bubble column contactor can for all intent and purposes be considered instantaneous and constant if the extraction efficiency is stable between bypasses (see empirical results below):

$$N_{fix_{AR}} = \frac{Q_{total}}{V} \left(\frac{\frac{1}{X} \frac{Q_{strip}}{Q_{total}} \left([C_2H_4]_{strip} - [C_2H_4]_{strip_0} e^{-\frac{Q_{total}\Delta t}{V}} \right)}{\left(1 - e^{-\frac{Q_{total}\Delta t}{V}} \right)} - b \right) \quad (9)$$

At steady-state (i.e. $t \rightarrow \infty$), Eq. (9) is identical to Eq. (2). For completion, we also present Eq. (9) with a correction for the dilution of the N_2 fixation signal associated with the addition of dissolved C_2H_4 using a correction factor of $\left(\frac{Q_{total}}{Q_{sw}}\right)$ and a conversion factor $\left(\frac{N_2}{C_2H_2}\right)$ for a final N_2 fixation rate (N_{fix}):

$$N_{fix} = \left(\frac{N_2}{C_2H_2}\right) \left(\frac{Q_{total}}{Q_{sw}}\right) \left(\frac{Q_{total}}{V}\right) \left(\frac{\frac{1}{X} \frac{Q_{strip}}{Q_{total}} \left([C_2H_4]_{strip} - [C_2H_4]_{strip_0} e^{-\frac{Q_{total}\Delta t}{V}} \right)}{\left(1 - e^{-\frac{Q_{total}\Delta t}{V}} \right)} - b \right) \quad (10)$$

An additional correction, not shown in Eq. (10) for clarity, is applied to $[C_2H_4]$ to account for the varying water vapor content, as measured by the CRDS, by normalizing the C_2H_4 gas mixing ratio to a dry gas mixing ratio (i.e. $[C_2H_4]_{dry} = (1 - r_{H_2O})^{-1} [C_2H_4]_{measured}$, where r_{H_2O} is the water vapor volume mixing ratio (v/v)).

Correction for ethylene contaminant in acetylene and natural background

1
2
3 In order to correct for temporal variations in background tracer C_2H_4 concentration (b factor in
4 Eq. (10)), instrumental drift and extraction efficiency, the following corrections are performed.
5
6 C_2H_2 is delivered at concentrations saturating the nitrogenase enzyme. The diazotrophic produc-
7 tion of C_2H_4 is therefore zeroth-order with respect to $[C_2H_2]$. In this regard, accurate delivery of
8 C_2H_2 gas is not critical. However, because of the non-negligible levels of C_2H_4 impurities in our
9 dissolved C_2H_2 solution, the admixing of C_2H_2 with the flowing seawater has to be highly repro-
10 ducible. C_2H_4 is also found naturally in surface waters due to biological and photochemical pro-
11 duction. For example, ethylene is produced during the bacterial degradation of phosphonates⁸⁹.
12 In surface waters of the North Atlantic subtropical gyre, the mean $[C_2H_4]$ is around 5 ± 3 ppb⁹⁰.
13 Similar concentrations are observed in other oligotrophic regions of the oceans⁹¹. Although we
14 are able to supply C_2H_2 reproducibly (see discussion below), and natural $[C_2H_4]$ and its variabil-
15 ity are relatively small, we take into account variations in the tracer b factor by having the sea-
16 water bypass the incubation chamber at regular intervals akin to a sample-standard bracketing
17 procedure. Such an approach also corrects for instrumental drift and varying extraction efficien-
18 cies. Under such conditions, $[C_2H_4]_{strip}$ reflects an incubation time which is for all intents and
19 purposes zero ($[C_2H_4]_{strip_{\tau=0}}$). In bypass mode, the $[C_2H_4]$ concentration in the stripping gas
20 will be close to steady-state after 3 to 4 e-folding residence time of the bubble column contactor.
21 Assuming steady-state and negligible acetylene reduction in bypass mode, the tracer b factor can
22 be derived from Eq. (10):
23
24
25
26
27
28
29
30
31
32
33
34
35
36
37
38
39
40
41
42
43
44
45
46
47

$$b = \frac{1}{X} \frac{Q_{strip}}{Q_{total}} [C_2H_4]_{strip_{\tau=0}} \quad (11)$$

48
49
50
51
52 In practice, we estimate the “ b ” factor at any time t as the temporal linear interpolation of the
53 bracketing bypass periods.
54
55
56
57
58
59
60

Method sensitivity and propagation of error

In order to propagate errors and assess the detection limit of FARACAS, we rearrange and combine Equations (2) and (11) for an estimate of the steady-state C_2H_2 reduction rate:

$$N_{fixAR} = \frac{Q_{strip}}{V} \frac{1}{X} \Delta[C_2H_4]_{strip} \quad (12)$$

where $(\Delta[C_2H_4]_{strip} = ([C_2H_4]_{strip} - [C_2H_4]_{strip\tau=0}))$. The modeled difference in C_2H_4 concentration between flow-through and bypass as a function of the stripping gas flow rate and the volume of the incubation chamber is presented in Fig. 3. A schematic illustration of a simulated FARACAS signal as a function of varying N_2 fixation rates is also shown in Fig. S3. Most of the parameters in Equation (12) are likely correlated. For example, variations in the stripping gas flow rate (Q_{strip}) introduce errors in the extraction efficiency (X) and the signal above background (i.e. $\Delta[C_2H_4]_{strip}$). However, as a first approximation, we propagate the errors assuming no covariance, in which case the relative error in N_{fixAR} ($\delta_{N_{fixAR}}$) is:

$$\frac{\delta_{N_{fixAR}}}{|N_{fixAR}|} = \sqrt{\left(\frac{\left((\delta_{[C_2H_4]_{strip}})^2 + (\delta_{[C_2H_4]_{strip}background})^2 \right)^{0.5}}{\Delta[C_2H_4]_{strip}} \right)^2 + \left(\frac{\delta_{Q_{strip}}}{Q_{strip}} \right)^2 + \left(\frac{\delta_X}{X} \right)^2} \quad (13)$$

With an estimated error of 0.6 ppb and 1 ppb for $(\delta_{[C_2H_4]_{strip}})$ and $(\delta_{[C_2H_4]_{strip}background})$ respectively (see empirical results below), and with the properties presented in Table 1,

$\frac{\delta_{N_{fixAR}}}{|N_{fixAR}|} = \left[\left(\frac{1.36}{\Delta[C_2H_4]_{strip}^2} \right) + 2 \times 10^{-4} + 2 \times 10^{-3} \right]^{0.5}$. Based on this equation, variations in the extraction efficiency introduce more error than changes in the stripping gas flow rate, further strengthening the argument for improving the extraction efficiency. The error in N_{fixAR} varies as a function of $\Delta[C_2H_4]_{strip}$. With $\Delta[C_2H_4]_{strip}$ increasing from 10 to 25 ppb, the relative error in N_{fixAR} de-

1
2
3 creases from 13 to 7%, at which point the error introduced by $\Delta[C_2H_4]_{strip}$ is as large as the one
4 associated with the extraction efficiency. The error increases rapidly at lower values being of
5 same magnitude as $N_{fix_{AR}}$ when $\Delta[C_2H_4]_{strip}$ is 1 ppb. As mentioned above, these calculations
6 should be interpreted with caution as they do not account for covariance. However, for an ap-
7 proximate context, the geometric mean (surface) volumetric N_2 fixation rates of 0.43 (0.71) nmol
8 $N L^{-1} d^{-1}$ presented in the meta-analysis of Luo et al.¹⁹ correspond to $\Delta[C_2H_4]_{strip}$ of 1.8 (3) ppb
9 with a FARACAS system with the properties as presented in Table 1.
10
11
12
13
14
15
16
17
18
19

20 As shown in Eq. (12), the detection limit of the FARACAS method depends on the ability to
21 detect a C_2H_4 signal above a background signal provided by the bypass. Applied to the FA-
22 RACAS method, the limit of detection (LoD) is the lowest concentration of C_2H_4 above the by-
23 pass signal (i.e. $\Delta[C_2H_4]_{strip}$) required to deduce the presence of N_2 fixation in the sample with
24 acceptable certainty. We note that precision and accuracy are generally poorly constrained at the
25 LoD⁹². Protocols for determining LoD commonly rely on visual evaluation, the standard devia-
26 tions or other statistical measures of the blank (here bypass) signal, the method's response and
27 the slope, or the signal-to-noise ratio (SNR)⁹³⁻⁹⁴. As each approach comes with drawbacks, there
28 is little consensus among the regulatory agencies and standards-setting organizations on a best
29 approach⁹⁵. A SNR of 2-3 has sometimes been recommended for the LoD. Based on this con-
30 vention, the N_2 fixation rates reported by Luo et al.¹⁹ are within the range of achievable meas-
31 urements with the CRDS considering the instrument has a precision of 0.2 ppb integrated over 5
32 min (3σ), and within the same order of magnitude as the stability of the flow-through and bypass
33 signals (see empirical results below). We think based on visual evaluation during our deploy-
34 ments at sea that a $\Delta[C_2H_4]_{strip}$ of 1 ppb can be reliably detected with the current configuration,
35 albeit with a significant uncertainty as discussed above, corresponding to N_2 fixation rates of
36
37
38
39
40
41
42
43
44
45
46
47
48
49
50
51
52
53
54
55
56
57
58
59
60

1
2
3 approximately 0.19 nmol N L⁻¹ d⁻¹. This is equivalent to or better than the sensitivity of most
4
5 current methods with a shorter time of incubation. For comparison, Montoya et al.⁷³ reported a
6
7 detection limit for the ¹⁵N₂ method of 0.48 nmol N L⁻¹ d⁻¹. Gradoville et al.⁹⁶ recently reported
8
9 averaged limits of detections of 0.21-1.09 nmol N L⁻¹ d⁻¹ and “minimal quantifiable rates” of
10
11 0.27-0.40 nmol N L⁻¹ d⁻¹. For deployments in regions with low N₂ fixation rates, the SNR of the
12
13 FARACAS method can be improved by increasing the extraction efficiency, or simply by
14
15 lengthening the flow-through incubation time (Fig. 3). In the same vein, the equations and theo-
16
17 retical considerations above also show that the FARACAS measurements reflect a time- and
18
19 space-averaged rate of N₂ fixation over the timescale of our incubations which can be shortened
20
21 in high N₂ fixation regions or by improving the C₂H₄ extraction efficiency (see section below on
22
23 extraction efficiency). Aliasing and smoothing could occur if the spatial and temporal variability
24
25 in N₂ fixation rates is at higher frequency than the flow-through incubation time. In its current
26
27 configuration, the FARACAS measurement frequency is well above the Nyquist frequency nec-
28
29 essary for capturing the diel cycle in N₂ fixation, as shown during our field deployments.
30
31
32
33
34
35

36 **Laboratory tests of the FARACAS method**

37 *Earlier work with gas standards and diazotrophic cultures*

38
39
40
41
42 Laboratory evaluations of the CRDS monitoring of ARA, including spectral interferences by
43
44 other gases such as C₂H₂ and CO₂, have been described in previous studies^{25,31}, where compari-
45
46 sons to the standard GC-FID approach were conducted with 1) varying concentrations of ultra-
47
48 high purity C₂H₄ certified standards (Airgas National Welders, Raleigh, NC, USA), and 2) diazo-
49
50 troph assemblages (mosses, lichens, and soil bacterial suspensions) at various stages of growth
51
52 and density and under a wide range of diazotrophic conditions.
53
54
55
56
57
58
59
60

1
2
3 CO₂ concentrations in surface waters vary substantially and could putatively interfere with C₂H₄
4 measurements. Negligible crosstalk from CO₂ was also documented over a wide range of CO₂
5 concentrations (380 - 20x10³ ppm), and the slight variations in [C₂H₂] during flow-through incu-
6 bations are unlikely to interfere with the C₂H₄ measurements. We also compared the CRDS
7 measurements to GC-FID on cultures of the marine diazotroph *Trichodesmium* (IMS101) in stat-
8 ic incubations with a closed-loop headspace in a configuration as in Cassar et al.²⁵ (Fig. S4).
9
10 Overall, these experiments show that the CRDS can measure C₂H₄ accurately with limited inter-
11 ference from C₂H₂ and CO₂.
12
13
14
15
16
17
18
19
20
21

22 ***Response time, stability of the signal, and gas extraction efficiency***

23
24
25 We empirically verified the response time of the bubble column contactor with step-tracer injec-
26 tion experiments, introducing water with different C₂H₄ concentrations into the column. Experi-
27 ments performed with Q_{strip} and V_{hs} of c. 28 mL min⁻¹ and 61 mL, respectively, led to an aver-
28 age e-folding response time of 114 seconds (Fig. S5), in line with theoretical predictions of 131
29 seconds for the e-folding response time of the headspace. This suggests that the turnover of the
30 headspace is likely a rate-determining step for the bubble column contactor. We do not need to
31 optimize this further as the overall response time of the bubble column contactor is much shorter
32 than the flow-through incubation time.
33
34
35
36
37
38
39
40
41
42
43

44 We tested the stability of the C₂H₄ signal measured by FARACAS with continuous admixing of
45 dissolved C₂H₂ with a water stream with constant C₂H₄ concentration. Averaged over 90 minutes
46 (i.e. e-folding incubation time in this current FARACAS configuration), the standard deviation
47 of the C₂H₄ signal in flow-through is less than 0.6 ppb. The standard deviation of the C₂H₄ signal
48 in bypass over 30 minutes is generally 0.5-1 ppb. The small difference in stability can likely be
49 attributed to the volume of the flow-through incubation dampening short-term fluctuations asso-
50 ciated with the flow-through incubation.
51
52
53
54
55
56
57
58
59
60

1
2
3 ciated with variability in the C₂H₄ contaminant delivery. We are currently exploring how subtle
4 changes in the gas flow rates and water level in the bubble column contactor, as recorded in
5 LabVIEW, may affect the stability of the C₂H₄ signal through its impact on the extraction effi-
6 ciency. Using C₂H₂ with less C₂H₄ contaminant would further reduce the high-frequency varia-
7 bility associated with delivery of the C₂H₂⁹⁷⁻⁹⁸. However, while such ultra-high-purity C₂H₂ gas-
8 es were at some point offered, they currently are not commercially available.

9
10
11
12
13
14
15
16
17
18 The extraction efficiency of the bubble column was determined by running C₂H₄ dissolved in
19 water through the bubble column contactor and collecting water downstream in a collapsible bag
20 and running it through the same contactor keeping all other water and gas flow rates constant. At
21 steady-state, the C₂H₄ concentration in the strip gas in the first run is equal to: $[C_2H_4]_{strip_1} =$
22 $\frac{Q_{total}}{Q_{strip}} X [C_2H_4]_{total}$. The C₂H₄ concentration downstream of the bubble column contactor reflects
23 what is left after the first run ($[C_2H_4]_{total}(1 - X)$). The C₂H₄ concentration in the strip gas dur-
24 ing the second run is therefore $[C_2H_4]_{strip_2} = \frac{Q_{total}}{Q_{strip}} X ([C_2H_4]_{total}(1 - X))$. Taking the ratio of
25 the two measurements and rearranging:
26
27
28
29
30
31
32
33
34
35
36
37

$$X = 1 - \frac{[C_2H_4]_{strip_2}}{[C_2H_4]_{strip_1}} \quad (14)$$

38
39
40
41
42
43 Based on these experiments, the average gas extraction efficiency is relatively constant at around
44 66% over a wide range of C₂H₄ concentrations (Table S1). We do not present the errors associat-
45 ed with these estimates as they are likely larger than the true reproducibility of the extraction
46 efficiency, as shown by the stability of the C₂H₄ signal (see discussion above on the stability of
47 the signal). We further verified the C₂H₄ recovery and the equations above with a pulse tracer
48 injection of a known amount of C₂H₄ in the flow-through incubator, thereby mimicking diazo-
49
50
51
52
53
54
55
56
57
58
59
60

1
2
3 trophic C₂H₂ reduction. The time-integrated C₂H₄ signal measured on the CRDS is consistent
4
5 with the C₂H₄ injected after accounting for the extraction efficiency (Fig. S6), further validating
6
7 the FARACAS method and the theoretical considerations about the kinetics described above and
8
9 in the supporting information. Overall, these experiments demonstrate that a constant [C₂H₄] can
10
11 be achieved with the dual-channel peristaltic pump admixing of dissolved C₂H₂ with seawater
12
13 and that the transfer coefficient at the bubble column contactor is stable and sufficient for our
14
15 purposes. However, the e-folding flow-through incubation time of 90 minutes in the current con-
16
17 figuration can be substantially reduced (i.e. smaller volume incubation chamber or higher sea-
18
19 water flow rate) by improving the extraction efficiency of the C₂H₄ gas in the bubble column
20
21 contactor. We tested the bottleneck or rate-limiting step to gas exchange by varying the water
22
23 and stripping gas flow rates with our current custom-made bubble column contactor. We found
24
25 that most of the resistance to mass transfer is associated with the stripping gas flow rate (Table
26
27 2), likely through its influence on the gas holdup. A tradeoff is therefore reached between in-
28
29 creasing the gas extraction kinetics ($k_L a V_l (1 - \varepsilon_g)$) by increasing Q_{strip} and diluting the C₂H₄
30
31 signal measured by the CRDS (Eq. 5). We are currently evaluating other C₂H₄ stripping designs,
32
33 including downflow and trickle-bed or packed bubble column contactors, heating of the bubble
34
35 column contactor, and the use of impellers to maintain small bubble size. The other approaches
36
37 tested thus far, including static mixers, spray-tower or showerhead and membrane contactors and
38
39 hybrids of these various approaches, did not significantly improve the extraction efficiency
40
41 and/or came with significant drawbacks (results not shown).
42
43
44
45
46
47
48
49

50 **Deployment of the FARACAS at sea for shipboard testing**

51
52 Field tests of the FARACAS method were conducted on the R/V *Atlantic Explorer* on three
53
54 cruises spanning a total of c.10,000 km of the Western North Atlantic. The cruise tracks were
55
56
57
58
59
60

1
2
3 selected in order to cover large gradients in N_2 fixation rates and covered the Sargasso Sea, a
4 region where oceanic N_2 fixation is believed to have a profound influence on the region's bioge-
5 ochemistry^{4, 37, 99}. These field campaigns were conducted in August based on the study of Orcutt
6 et al.¹⁰⁰ which showed N_2 fixation rates peaking at the end of the summer in the region. A por-
7 tion of the transect is presented in Fig. 4 with the scientific findings from these deployments fur-
8 ther discussed in the recent study of Tang et al.¹⁰¹. Briefly, N_2 fixation rates were found to be
9 highest in waters on the American Atlantic continental shelf, challenging classical views on oce-
10 anic N_2 fixation biogeography. During one of these cruises, we compared the light field emulated
11 in the flow-through incubation chamber to Photosynthetically Active Radiation (PAR) as meas-
12 ured on a mast on the ship. While PAR shows more day-to-day variability because of variable
13 cloud cover, the diel cycles of light availability are well reproduced in our flow-through incuba-
14 tion chamber (Fig. S7). Although our observations integrated over the timescale of our flow-
15 through incubations do not show variability in N_2 fixation rates as a function of varying cloud
16 cover, we are currently exploring the possibility of using PAR sensors to adjust in real-time the
17 light regime in the flow-through incubation chamber.

18
19 Discrete ^{15}N tracer incubations following the protocol of Mohr et al.⁷⁸ were performed concu-
20 rrently with the deployment of FARACAS. For comparison, our measurements can be integrated
21 over 24 hrs to derive daily N_2 fixation using a moving average, integrating the area under the
22 curve, or simulating the daily cycle centered at the N_2 fixation maximum. Our results show a
23 relatively good agreement to this benchmark method assuming a C_2H_2 to N_2 conversion ratio of
24 4:1^{73-74, 102} (Fig. 5). A perfect match to the ^{15}N incubations is not expected for the various rea-
25 sons enumerated in the section on "Current methods for measuring N_2 fixation rates" (e.g. vary-
26 ing C_2H_2/N_2 stoichiometry), and the fact that our observations were not Lagrangian. As opposed
27
28
29
30
31
32
33
34
35
36
37
38
39
40
41
42
43
44
45
46
47
48
49
50
51
52
53
54
55
56
57
58
59
60

1
2
3 to discrete measurements, our observations integrate over temporal as well as spatial scales. At
4
5 most locations, we were not on station for a full 24 hr. The agreement to the ^{15}N incubations is
6
7 best where we have observations over a nearly-full diel cycle.
8
9

10 **Limitations of the FARACAS method**

11
12
13 The method relies on the surrogate reaction of C_2H_2 reduction to estimate N_2 fixation. As men-
14
15 tioned above, the C_2H_2 to N_2 conversion stoichiometry has been found to be variable e.g., ⁶⁷.
16
17 Therefore, as is the case with the conventional GC-FID detection of ARA, FARACAS ultimately
18
19 requires calibration of the $\text{C}_2\text{H}_2/\text{N}_2$ conversion factor by comparison to the ^{15}N tracer incubations
20
21 on discrete samples ^{4-5, 63, 73, 103}. In our study, we found a good correlation of FARACAS to ^{15}N
22
23 tracer incubations.
24
25
26

27
28 In the current configuration, the method reflects surface volumetric N_2 fixation rates at a fixed
29
30 underway depth of approximately 3 meters. As is the case with the other methods which rely on
31
32 CTD sampling, our approach does not sample the very-surface which can harbor a thriving dia-
33
34 zotrophic community such as floating *Trichodesmium* colonies. In some cases, N_2 fixation rates
35
36 integrated over the entire water column may also be more desirable. In this regard, we note that
37
38 most of the N_2 fixation generally occurs at the surface, and that depth-integrated N_2 fixation rates
39
40 are often proportional to the surface volumetric N_2 fixation rates (Fig. S8). Moreover, the repre-
41
42 sentativeness of our underway fixed-depth measurements can be evaluated, and the vertical dis-
43
44 tribution of N_2 fixation rates can be studied at high resolution with the deployment of an adjusta-
45
46 ble-depth towfish (e.g. Chelsea' SeaSoar, SeaSciences's Acrobat, Wetlabs' Dolphin, or MacArt-
47
48 ney's Triaxus).
49
50
51
52

53 **Advantages of the FARACAS method**

1
2
3 Traditional methods require long incubations which may exacerbate bottle artefacts including
4 changes in microbial community structure and metabolic activity ⁶⁴. Some of the traditional
5 methods also require pre-concentration of cells in order to increase the signal ⁹⁸, which selects
6 for a portion of the diazotrophic community and may damage cells or modify their physiology.
7
8 The high sensitivity of the FARACAS method limits such issues by not requiring preconcentra-
9 tion of cells and reducing the incubations time.
10
11

12
13
14
15
16
17 As importantly, the continuous measurements provided by the FARACAS method allow for
18 adaptive sampling and better capture the spatial and temporal heterogeneity of N₂ fixation. Karl
19 et al. ¹⁷ pointed out that “N₂ fixation in the sea probably occurs during stochastic, heterogeneous
20 blooms that are not easily predicted or resolved,” and added that “scientists ... rarely produce
21 data sets that can be statistically scaled to an unbiased average value for a particular biome” see
22 also ¹⁹. This is critical because an increasing number of studies have demonstrated that account-
23 ing for rare episodic events and intricate mesoscale and submesoscale processes is important to
24 closing biogeochemical budgets at the ocean surface ¹⁰⁴⁻¹⁰⁹. High-resolution sampling of multiple
25 biomes will also improve the statistical inferences used to further disentangle the controls on N₂
26 fixation rates and assess how they relate to carbon cycling ¹⁰¹. Finally, FARACAS provides a
27 unique opportunity to investigate the diel periodicity (i.e. circadian rhythm) of N₂ fixation, as
28 illustrated in Fig. 4.
29
30
31
32
33
34
35
36
37
38
39
40
41
42
43
44

45 **Conclusions**

46
47
48 In the FARACAS method, the surrogate reaction of C₂H₂ to C₂H₄ conventionally used to esti-
49 mate N₂ fixation is unchanged, but measurements are made instantaneously and continuously at
50 ppb levels, allowing for high-resolution underway observations. Because of the high sensitivity
51 of our method, the flow-through incubation time can be short without preconcentration of cells,
52
53
54
55
56
57
58
59
60

1
2
3 thereby limiting artefacts associated with sample handling, delays in processing, and long-term
4 incubations. The FARACAS method opens numerous research directions pertaining to diazotro-
5 phy in freshwater and marine systems, and can be adapted for measuring other biological rate
6 processes. With the pervasive anthropogenic disturbance of climate, including desertification and
7 altered dust sources, and the perturbation of the nitrogen cycle, it is imperative to better charac-
8 terize the current variability and the global habitat of N₂ fixation. Our new method complements
9 the broad array of observational, geochemical tracer, molecular, remote sensing and modeling
10 approaches that can be used to assess the current state of oceanic nitrogen cycling and monitor
11 future changes.
12
13
14
15
16
17
18
19
20
21
22

23 24 **V. ACKNOWLEDGEMENTS**

25
26 We thank Geoffrey Smith (UCSC) for help with the construction and field deployment of the
27 towfish in the first year of this project. We are very grateful to Rod Johnson, the Bermuda Insti-
28 tute of Ocean Sciences, and the crew of the R/V Atlantic Explorer for their invaluable support
29 during our field trials of the FARACAS method on three research cruises. We also thank Hugo
30 Berthelot (UBO), Debany Fonseca Batista and Frank Dehairs (AMGC, Vrije Universiteit Brus-
31 sel) for conducting the dissolved ¹⁵N₂ incubations and sharing their results, and Hans Pearl
32 (UNC) for providing *Trichodesmium* cultures. This work was funded by an NSF-CAREER grant
33 (3331939) to N. C. and a Link Foundation Ocean Engineering & Instrumentation Fellowship to
34 W. T. N. C. was also in part supported by a North Carolina Sea Grant (2014-1920-18), and the
35 "Laboratoire d'Excellence" LabexMER (ANR-10-LABX-19), co-funded by a grant from the
36 French government under the program "Investissements d'Avenir".
37
38
39
40
41
42
43
44
45
46
47
48
49
50
51
52
53
54
55
56
57
58
59
60

VI. REFERENCES

1. J. P. Zehr, E. J. Carpenter, T. A. Villareal, New perspectives on nitrogen-fixing microorganisms in tropical and subtropical oceans. *Trends Microbiol* 2000, 8. 68-73.
2. R. J. Langlois, J. LaRoche, P. A. Raab, Diazotrophic diversity and distribution in the tropical and subtropical Atlantic ocean. *Appl Environ Microb* 2005, 71. 7910-7919, DOI: Doi 10.1128/Aem.71.12.7910-7919.2005.
3. K. Fennel, Y. H. Spitz, R. M. Letelier, M. R. Abbott, D. M. Karl, A deterministic model for N₂ fixation at stn. ALOHA in the subtropical North Pacific Ocean. *Deep-Sea Res Pt II* 2002, 49. 149-174.
4. D. G. Capone, J. A. Burns, J. P. Montoya, A. Subramaniam, C. Mahaffey, T. Gunderson, A. F. Michaels, E. J. Carpenter, Nitrogen fixation by *Trichodesmium* spp.: An important source of new nitrogen to the tropical and subtropical North Atlantic Ocean. *Global Biogeochem Cy* 2005, 19. DOI: Artn Gb2024
Doi 10.1029/2004gb002331.
5. C. Mahaffey, A. F. Michaels, D. G. Capone, The conundrum of marine N₂ fixation. *Am J Sci* 2005, 305. 546-595.
6. P. G. Falkowski, Evolution of the nitrogen cycle and its influence on the biological sequestration of CO₂ in the ocean. *Nature* 1997, 387. 272-275.
7. S. A. Sanudo-Wilhelmy, A. B. Kustka, C. J. Gobler, D. A. Hutchins, M. Yang, K. Lwiza, J. Burns, D. G. Capone, J. A. Raven, E. J. Carpenter, Phosphorus limitation of nitrogen fixation by *Trichodesmium* in the central Atlantic Ocean. *Nature* 2001, 411. 66-69.
8. J. Wu, W. Sunda, E. A. Boyle, D. M. Karl, Phosphate depletion in the Western North Atlantic Ocean. *Science* 2000, 289. 759-762.
9. M. M. Mills, C. Ridame, M. Davey, J. La Roche, R. J. Geider, Iron and phosphorus co-limit nitrogen fixation in the eastern tropical North Atlantic. *Nature* 2004, 429. 292-294, DOI: Doi 10.1038/Nature02550.
10. I. Berman-Frank, J. T. Cullen, Y. Shaked, R. M. Sherrell, P. G. Falkowski, Iron availability, cellular iron quotas, and nitrogen fixation in *Trichodesmium*. *Limnol Oceanogr* 2001, 46. 1249-1260.
11. R. M. Moore, S. Punshon, C. Mahaffey, D. Karl, The relationship between dissolved hydrogen and nitrogen fixation in ocean waters. *Deep-Sea Res Pt I* 2009, 56. 1449-1458, DOI: DOI 10.1016/j.dsr.2009.04.008.
12. M. Rubin, I. Berman-Frank, Y. Shaked, Dust- and mineral-iron utilization by the marine dinitrogen-fixer *Trichodesmium*. *Nat Geosci* 2011, 4. 529-534, DOI: Doi 10.1038/Ngeo1181.
13. M. M. Mills, K. R. Arrigo, Magnitude of oceanic nitrogen fixation influenced by the nutrient uptake ratio of phytoplankton. *Nat Geosci* 2010, 3. 412-416, DOI: Doi 10.1038/Ngeo856.
14. T. Y. Ho, Nickel limitation of nitrogen fixation in *Trichodesmium*. *Limnol Oceanogr* 2013, 58. 112-120, DOI: DOI 10.4319/lo.2013.58.1.0112.
15. Y. W. Luo, I. D. Lima, D. M. Karl, C. A. Deutsch, S. C. Doney, Data-based assessment of environmental controls on global marine nitrogen fixation. *Biogeosciences* 2014, 11. 691-708, DOI: 10.5194/bg-11-691-2014.

- 1
2
3 16. T. Weber, C. Deutsch, Local versus basin-scale limitation of marine nitrogen fixation. *P Natl Acad Sci USA* 2014, *111*. 8741-8746, DOI: 10.1073/pnas.1317193111.
4
5
6 17. D. Karl, A. Michaels, B. Bergman, D. Capone, E. Carpenter, R. Letelier, F. Lipschultz, H. Paerl,
7 D. Sigman, L. Stal, Dinitrogen fixation in the world's oceans. *Biogeochemistry* 2002, *57*. 47-+.
- 8 18. J. P. Zehr, Nitrogen fixation by marine cyanobacteria. *Trends Microbiol* 2011, *19*. 162-173, DOI:
9 DOI 10.1016/j.tim.2010.12.004.
10
- 11 19. Y. W. Luo, S. C. Doney, L. A. Anderson, M. Benavides, A. Bode, S. Bonnet, K. H. Boström, D.
12 Böttjer, D. G. Capone, E. J. Carpenter, Y. L. Chen, M. J. Church, J. E. Dore, L. I. Falcón, A. Fernández,
13 R. A. Foster, K. Furuya, F. Gómez, K. Gundersen, A. M. Hynes, D. M. Karl, S. Kitajima, R. J. Langlois,
14 J. LaRoche, R. M. Letelier, E. Marañón, D. J. McGillicuddy Jr, P. H. Moisander, C. M. Moore, B.
15 Mouriño-Carballido, M. R. Mulholland, J. A. Needoba, K. M. Orcutt, A. J. Poulton, P. Raimbault, A. P.
16 Rees, L. Riemann, T. Shiozaki, A. Subramaniam, T. Tyrrell, K. A. Turk-Kubo, M. Varela, T. A. Villareal,
17 E. A. Webb, A. E. White, J. Wu, J. P. Zehr, Database of diazotrophs in global ocean: abundances,
18 biomass and nitrogen fixation rates. *Earth Syst. Sci. Data Discuss.* 2012, *5*. 47-106, DOI: 10.5194/essdd-
19 5-47-2012.
20
- 21 20. C. J. Somes, A. Oschlies, A. Schmittner, Isotopic constraints on the pre-industrial oceanic
22 nitrogen budget. *Biogeosciences* 2013, *10*. 5889-5910, DOI: 10.5194/bg-10-5889-2013.
23
- 24 21. M. Benavides, M. Voss, Five decades of N₂ fixation research in the North Atlantic Ocean.
25 *Frontiers in Marine Science* 2015, *2*. DOI: 10.3389/fmars.2015.00040.
- 26 22. N. Gruber, Elusive marine nitrogen fixation. *P Natl Acad Sci USA* 2016, *113*. 4246-4248, DOI:
27 10.1073/pnas.1603646113.
28
- 29 23. W. D. P. Stewart, Fitzgera.Gp, R. H. Burris, In Situ Studies on N₂ fixation Using Acetylene
30 Reduction Technique. *P Natl Acad Sci USA* 1967, *58*. 2071-2078.
- 31 24. R. Schöllhorn, R. H. Burris, Acetylene as a Competitive Inhibitor of N₂ Fixation. *P Natl Acad Sci*
32 *USA* 1967, *58*. 213-&.
33
- 34 25. N. Cassar, J. P. Bellenger, R. B. Jackson, J. Karr, B. A. Barnett, N₂ fixation estimates in real-time
35 by cavity ring-down laser absorption spectroscopy. *Oecologia* 2012, *168*. 335-42, DOI: 10.1007/s00442-
36 011-2105-y.
37
- 38 26. K. W. Bruland, E. L. Rue, G. J. Smith, G. R. DiTullio, Iron, macronutrients and diatom blooms in
39 the Peru upwelling regime: brown and blue waters of Peru. *Mar Chem* 2005, *93*. 81-103, DOI:
40 10.1016/j.marchem.2004.06.011.
- 41 27. L. D. Pickell, M. L. Wells, C. G. Trick, W. P. Cochlan, A sea-going continuous culture system
42 for investigating phytoplankton community response to macro- and micro-nutrient manipulations. *Limnol*
43 *Oceanogr-Meth* 2009, *7*. 21-32.
44
- 45 28. T. J. Browning, H. A. Bouman, C. M. Moore, C. Schlosser, G. A. Tarran, E. M. S. Woodward, G.
46 M. Henderson, Nutrient regimes control phytoplankton ecophysiology in the South Atlantic.
47 *Biogeosciences* 2014, *11*. 463-479, DOI: 10.5194/bg-11-463-2014.
48
- 49 29. H. X. Xie, O. C. Zafiriou, W. Wang, C. D. Taylor, A simple automated continuous flow
50 equilibration method for measuring carbon monoxide in seawater. *Environ Sci Technol* 2001, *35*. 1475-
51 1480, DOI: DOI 10.1021/es001656v.
- 52 30. L. E. Rafelski, B. Paplawsky, R. F. Keeling, An Equilibrator System to Measure Dissolved
53 Oxygen and Its Isotopes. *J Atmos Ocean Tech* 2013, *30*. 361-377, DOI: 10.1175/Jtech-D-12-00074.1.
54
- 55 31. M.-E. Jean, N. Cassar, C. Setzer, B. A. Barnett, J. P. Bellenger, Short-term N₂ fixation kinetics in
56 a moss-associated cyanobacteria. *Environmental Science and Technology* 2012, *46*. 8667-8671.
57
58
59
60

- 1
2
3 32. P. G. Falkowski, R. T. Barber, V. Smetacek, Biogeochemical controls and feedbacks on ocean
4 primary production. *Science* 1998, *281*. 200-206.
5
6 33. J. N. Galloway, F. J. Dentener, D. G. Capone, E. W. Boyer, R. W. Howarth, S. P. Seitzinger, G.
7 P. Asner, C. C. Cleveland, P. A. Green, E. A. Holland, D. M. Karl, A. F. Michaels, J. H. Porter, A. R.
8 Townsend, C. J. Vorosmarty, Nitrogen cycles: past, present, and future. *Biogeochemistry* 2004, *70*. 153-
9 226.
10
11 34. D. Karl, R. Letelier, L. Tupas, J. Dore, J. Christian, D. Hebel, The role of nitrogen fixation in
12 biogeochemical cycling in the subtropical North Pacific Ocean. *Nature* 1997, *388*. 533-538.
13
14 35. D. G. Capone, D. A. Bronk, M. R. Mulholland, E. J. Carpenter, *Nitrogen in the Marine*
15 *Environment*. Academic: San Diego, 2008; p 1757.
16
17 36. D. M. Karl, M. J. Church, J. E. Dore, R. M. Letelier, C. Mahaffey, Predictable and efficient
18 carbon sequestration in the North Pacific Ocean supported by symbiotic nitrogen fixation. *P Natl Acad*
19 *Sci USA* 2012, doi: 10.1073/pnas.1120312109.
20
21 37. K. Lee, D. M. Karl, R. Wanninkhof, J. Z. Zhang, Global estimates of net carbon production in the
22 nitrate-depleted tropical and subtropical oceans. *Geophys Res Lett* 2002, *29*. -.
23
24 38. T. Shiozaki, T. Kodama, S. Kitajima, M. Sato, K. Furuya, Advective transport of diazotrophs and
25 importance of their nitrogen fixation on new and primary production in the western Pacific warm pool.
26 *Limnol Oceanogr* 2013, *58*. 49-60, DOI: DOI 10.4319/lo.2013.58.1.0049.
27
28 39. V. J. Coles, R. R. Hood, M. Pascual, D. G. Capone, Modeling the impact of Trichodesmium and
29 nitrogen fixation in the Atlantic Ocean. *J Geophys Res-Oceans* 2004, *109*. DOI: Artn C06007
30 Doi 10.1029/2002jc001754.
31
32 40. S. Bonnet, I. C. Biegala, P. Dutrieux, L. O. Slemmons, D. G. Capone, Nitrogen fixation in the
33 western equatorial Pacific: Rates, diazotrophic cyanobacterial size class distribution, and biogeochemical
34 significance. *Global Biogeochem Cy* 2009, *23*. DOI: Artn Gb3012
35 Doi 10.1029/2008gb003439.
36
37 41. J. P. Zehr, J. B. Waterbury, P. J. Turner, J. P. Montoya, E. Omoregie, G. F. Steward, A. Hansen,
38 D. M. Karl, Unicellular cyanobacteria fix N₂ in the subtropical North Pacific Ocean. *Nature* 2001, *412*.
39 635-638.
40
41 42. M. J. Church, K. M. Bjorkman, D. M. Karl, M. A. Saito, J. P. Zehr, Regional distributions of
42 nitrogen-fixing bacteria in the Pacific Ocean. *Limnol Oceanogr* 2008, *53*. 63-77.
43
44 43. J. A. Sohm, A. Subramaniam, T. E. Gunderson, E. J. Carpenter, D. G. Capone, Nitrogen fixation
45 by Trichodesmium spp. and unicellular diazotrophs in the North Pacific Subtropical Gyre. *J Geophys Res-*
46 *Biogeo* 2011, *116*. DOI: Artn G03002
47 Doi 10.1029/2010jg001513.
48
49 44. P. H. Moisander, R. A. Beinart, I. Hewson, A. E. White, K. S. Johnson, C. A. Carlson, J. P.
50 Montoya, J. P. Zehr, Unicellular Cyanobacterial Distributions Broaden the Oceanic N₂ Fixation Domain.
51 *Science* 2010, *327*. 1512-1514, DOI: DOI 10.1126/science.1185468.
52
53 45. H. Halm, P. Lam, T. G. Ferdelman, G. Lavik, T. Dittmar, J. LaRoche, S. D'Hondt, M. M. M.
54 Kuypers, Heterotrophic organisms dominate nitrogen fixation in the South Pacific Gyre. *Isme J* 2012, *6*.
55 1238-1249, DOI: 10.1038/ismej.2011.182.
56
57 46. T. Shiozaki, M. Ijichi, T. Kodama, S. Takeda, K. Furuya, Heterotrophic bacteria as major
58 nitrogen fixers in the euphotic zone of the Indian Ocean. *Global Biogeochem Cy* 2014, *28*. 1096-1110,
59 DOI: 10.1002/2014gb004886.
60

- 1
2
3 47. M. Bentzon-Tilia, I. Severin, L. H. Hansen, L. Riemann, Genomics and Ecophysiology of
4 Heterotrophic Nitrogen-Fixing Bacteria Isolated from Estuarine Surface Water. *Mbio* 2015, 6. DOI:
5 ARTN e00929-15
6
7 10.1128/mBio.00929-15.
8
9 48. F. M. Monteiro, M. J. Follows, S. Dutkiewicz, Distribution of diverse nitrogen fixers in the global
10 ocean. *Global Biogeochem Cy* 2010, 24. DOI: Artn Gb3017
11 Doi 10.1029/2009gb003731.
12
13 49. L. Guidi, P. H. R. Calil, S. Duhamel, K. M. Björkman, S. C. Doney, G. A. Jackson, B. Li, M. J.
14 Church, S. Tozzi, Z. S. Kolber, K. J. Richards, A. A. Fong, R. M. Letelier, G. Gorsky, L. Stemmann, D.
15 M. Karl, Does eddy-eddy interaction control surface phytoplankton distribution and carbon export in the
16 North Pacific Subtropical Gyre? *J. Geophys. Res.* 2012, 117. G02024, DOI: 10.1029/2012jg001984.
17
18 50. E. J. Carpenter, D. G. Capone, in *Nitrogen in the Marine Environment*, ed. D. G. C. e. al.
19 Academic: San Diego, Calif., 2008, vol. doi:10.1016/B978-0-12-372522-6.00004-9, pp 141–198.
20
21 51. C. Deutsch, J. L. Sarmiento, D. M. Sigman, N. Gruber, J. P. Dunne, Spatial coupling of nitrogen
22 inputs and losses in the ocean. *Nature* 2007, 445. 163-167.
23
24 52. D. G. Capone, J. P. Zehr, H. W. Paerl, B. Bergman, E. J. Carpenter, Trichodesmium, a globally
25 significant marine cyanobacterium. *Science* 1997, 276. 1221-1229.
26
27 53. N. Gruber, J. L. Sarmiento, Global patterns of marine nitrogen fixation and denitrification. *Global*
28 *Biogeochem Cy* 1997, 11. 235-266.
29
30 54. D. A. Hansell, N. R. Bates, D. B. Olson, Excess nitrate and nitrogen fixation in the North Atlantic
31 Ocean. *Mar Chem* 2004, 84. 243-265, DOI: DOI 10.1016/j.marchem.2003.08.004.
32
33 55. A. Landolfi, A. Oschlies, R. Sanders, Organic nutrients and excess nitrogen in the North Atlantic
34 subtropical gyre. *Biogeosciences* 2008, 5. 1199-1213.
35
36 56. J. K. Moore, S. C. Doney, K. Lindsay, N. Mahowald, A. F. Michaels, Nitrogen fixation amplifies
37 the ocean biogeochemical response to decadal timescale variations in mineral dust deposition. *Tellus B*
38 2006, 58. 560-572.
39
40 57. J. P. Zehr, R. M. Kudela, Nitrogen Cycle of the Open Ocean: From Genes to Ecosystems. *Annu*
41 *Rev Mar Sci* 2011, 3. 197-225, DOI: DOI 10.1146/annurev-marine-120709-142819.
42
43 58. M. J. Dilworth, Acetylene Reduction by Nitrogen-Fixing Preparations from *Clostridium*
44 *Pasteurianum*. *Biochimica Et Biophysica Acta* 1966, 127. 285-&.
45
46 59. B. Koch, H. J. Evans, S. Russell, Reduction of Acetylene and Nitrogen Gas by Breis and Cell-
47 Free Extracts of Soybean Root Nodules. *Plant Physiol* 1967, 42. 466-468.
48
49 60. B. Koch, H. J. Evans, Reduction of Acetylene to Ethylene by Soybean Root Nodules. *Plant*
50 *Physiol* 1966, 41. 1748-1750.
51
52 61. R. W. F. Hardy, R. D. Holsten, E. K. Jackson, R. C. Burns, Acetylene-Ethylene Assay for N₂
53 Fixation - Laboratory and Field Evaluation. *Plant Physiol* 1968, 43. 1185-&.
54
55 62. R. S. Oremland, D. G. Capone, Use of Specific Inhibitors in Biogeochemistry and Microbial
56 Ecology. *Adv Microb Ecol* 1988, 10. 285-383.
57
58 63. D. G. Capone, in *Handbook of methods in aquatic microbial ecology*, ed. B. S. P. F. Kemp, E.
59 Sherr and J. Cole. Lewis Publishers, 1993, pp 621-631.
60

- 1
2
3 64. R. W. Fulweiler, E. M. Heiss, M. K. Rogener, S. E. Newell, G. R. LeClerc, S. M. Kortebein, S.
4 W. Wilhelm, Examining the impact of acetylene on N-fixation and the active sediment microbial
5 community. *Front Microbiol* 2015, 6. DOI: ARTN 418
6 10.3389/fmicb.2015.00418.
7
8 65. H. Zuckermann, M. Staal, L. J. Stal, J. Reuss, S. T. L. Hekkert, F. Harren, D. Parker, On-line
9 monitoring of nitrogenase activity in cyanobacteria by sensitive laser photoacoustic detection of ethylene.
10 *Appl Environ Microb* 1997, 63. 4243-4251.
11
12 66. S. T. te Lintel Hekkert, M. J. Staal, R. H. M. Nabben, H. Zuckermann, S. Persijn, L. J. Stal, L. A.
13 C. J. Voesenek, F. J. M. Harren, J. Reuss, D. H. Parker, Laser photoacoustic trace gas detection, an
14 extremely sensitive technique applied in biological research. *Instrumentation Science & Technology*
15 1998, 26. 157-175.
16
17 67. S. T. Wilson, D. Bottjer, M. J. Church, D. M. Karl, Comparative Assessment of Nitrogen
18 Fixation Methodologies, Conducted in the Oligotrophic North Pacific Ocean. *Appl Environ Microb* 2012,
19 78. 6516-6523, DOI: Doi 10.1128/Aem.01146-12.
20
21 68. M. Staal, S. T. Lintel-Hekkert, F. Harren, L. Stal, Nitrogenase activity in cyanobacteria measured
22 by the acetylene reduction assay: a comparison between batch incubation and on-line monitoring. *Environ*
23 *Microbiol* 2001, 3. 343-351.
24
25 69. J. P. Houchins, The Physiology and Biochemistry of Hydrogen Metabolism in Cyanobacteria.
26 *Biochimica Et Biophysica Acta* 1984, 768. 227-255.
27
28 70. J. Kim, D. C. Rees, Nitrogenase and Biological Nitrogen-Fixation. *Biochemistry-Us* 1994, 33.
29 389-397.
30
31 71. J. S. Kim, D. C. Rees, Crystallographic Structure and Functional Implications of the Nitrogenase
32 Molybdenum Iron Protein from *Azotobacter-Vinelandii*. *Nature* 1992, 360. 553-560.
33
34 72. R. B. Peterson, R. H. Burris, Conversion of Acetylene-Reduction Rates to Nitrogen-Fixation
35 Rates in Natural-Populations of Blue-Green-Algae. *Analytical Biochemistry* 1976, 73. 404-410.
36
37 73. J. P. Montoya, M. Voss, P. Kahler, D. G. Capone, A simple, high-precision, high-sensitivity
38 tracer assay for N₂ fixation. *Appl Environ Microb* 1996, 62. 986-993.
39
40 74. M. R. Mulholland, D. A. Bronk, D. G. Capone, Dinitrogen fixation and release of ammonium and
41 dissolved organic nitrogen by *Trichodesmium* IMS101. *Aquat Microb Ecol* 2004, 37. 85-94.
42
43 75. H. Berthelot, M. Benavides, P. H. Moisaner, O. Grosso, S. Bonnet, High-nitrogen fixation rates
44 in the particulate and dissolved pools in the Western Tropical Pacific (Solomon and Bismarck Seas).
45 *Geophys Res Lett* 2017. n/a-n/a, DOI: 10.1002/2017GL073856.
46
47 76. U. Konno, U. Tsunogai, D. D. Komatsu, S. Daita, F. Nakagawa, A. Tsuda, T. Matsui, Y. J. Eum,
48 K. Suzuki, Determination of total N₂ fixation rates in the ocean taking into account both the particulate
49 and filtrate fractions. *Biogeosciences* 2010, 7. 2369-2377, DOI: 10.5194/bg-7-2369-2010.
50
51 77. W. J. Payne, Influence of Acetylene on Microbial and Enzymatic Assays. *J Microbiol Meth* 1984,
52 2. 117-133, DOI: Doi 10.1016/0167-7012(84)90001-0.
53
54 78. W. Mohr, T. Grosskopf, D. W. R. Wallace, J. LaRoche, Methodological Underestimation of
55 Oceanic Nitrogen Fixation Rates. *Plos One* 2010, 5. DOI: ARTN e12583
56 DOI 10.1371/journal.pone.0012583.
57
58 79. R. Dabundo, M. F. Lehmann, L. Treibergs, C. R. Tobias, M. A. Altabet, P. H. Moisaner, J.
59 Granger, The contamination of ¹⁵N₂ gas stocks with ¹⁵N-labeled nitrate and ammonium and consequences
60 for nitrogen fixation measurements. *Plos One* 2014, 9. e110335, DOI: 10.1371/journal.pone.0110335.

- 1
2
3 80. N. Kantarci, F. Borak, K. O. Ulgen, Bubble column reactors. *Process Biochem* 2005, 40. 2263-
4 2283, DOI: 10.1016/j.procbio.2004.10.004.
5
6 81. N. G. Deen, R. F. Mudde, J. A. M. Kuipers, P. Zehner, M. Kraume, in *Ullmann's Encyclopedia of*
7 *Industrial Chemistry*. Wiley-VCH Verlag GmbH & Co. KGaA, 2000.
8
9 82. R. Krishna, J. M. van Baten, Mass transfer in bubble columns. *Catal Today* 2003, 79. 67-75,
10 DOI: 10.1016/S0920-5861(03)00046-4.
11
12 83. A. Behkish, Z. W. Men, J. R. Inga, B. I. Morsi, Mass transfer characteristics in a large-scale
13 slurry bubble column reactor with organic liquid mixtures. *Chem Eng Sci* 2002, 57. 3307-3324, DOI: Pii
14 S0009-2509(02)00201-4
15 Doi 10.1016/S0009-2509(02)00201-4.
16
17 84. S. S. Alves, S. P. Orvalho, J. M. T. Vasconcelos, Effect of bubble contamination on rise velocity
18 and mass transfer. *Chem Eng Sci* 2005, 60. 1-9, DOI: <https://doi.org/10.1016/j.ces.2004.07.053>.
19
20 85. C. R. Wilke, P. Chang, Correlation of Diffusion Coefficients in Dilute Solutions. *Aiche J* 1955, 1.
21 264-270.
22
23 86. D. B. King, W. J. De Bruyn, M. Zheng, E. S. Saltzman, in *Air-Water Gas Transfer*, ed. B. J. a. E.
24 C. Monahan. AEON Verlag and Studio: Hanau, 1996.
25
26 87. R. J. Flett, R. D. Hamilton, N. E. R. Campbell, Aquatic Acetylene-Reduction Techniques -
27 Solutions to Several Problems. *Can J Microbiol* 1976, 22. 43-51.
28
29 88. E. Breitbarth, M. M. Mills, G. Friedrichs, J. LaRoche, The Bunsen gas solubility coefficient of
30 ethylene as a function of temperature and salinity and its importance for nitrogen fixation assays. *Limnol*
31 *Oceanogr-Meth* 2004, 2. 282-288.
32
33 89. O. A. Sosa, D. J. Repeta, S. Ferron, J. A. Bryant, D. R. Mende, D. M. Karl, E. F. DeLong,
34 Isolation and Characterization of Bacteria That Degrade Phosphonates in Marine Dissolved Organic
35 Matter. *Front Microbiol* 2017, 8. DOI: ARTN 1786
36 10.3389/fmicb.2017.01786.
37
38 90. R. Seifert, N. Delling, H. H. Richnow, S. Kempe, J. Hefter, W. Michaelis, Ethylene and methane
39 in the upper water column of the subtropical Atlantic. *Biogeochemistry* 1999, 44. 73-91.
40
41 91. J. W. Swinnerton, R. A. Lamontagne, Oceanic Distribution of Low-Molecular-Weight
42 Hydrocarbons - Baseline Measurements. *Environ Sci Technol* 1974, 8. 657-663.
43
44 92. D. A. Armbruster, T. Pry, Limit of Blank, Limit of Detection and Limit of Quantitation. *The*
45 *Clinical Biochemist Reviews* 2008, 29. S49-S52.
46
47 93. T. A. Little, Method Validation Essentials, Limit of Blank, Limit of Detection, and Limit of
48 Quantitation. *Biopharm Int* 2015, 28. 48-51.
49
50 94. S. G. Huang, T. H. Wang, M. Yang, The Evaluation of Statistical Methods for Estimating the
51 Lower Limit of Detection. *Assay Drug Dev Techn* 2013, 11. 35-43, DOI: 10.1089/adt.2011.438.
52
53 95. A. Shrivastava, V. B. Gupta, Methods for the determination of limit of detection and limit of
54 quantitation of the analytical methods. *Chronicles of Young Scientists* 2011, 2. 21-25, DOI:
55 10.4103/2229-5186.79345.
56
57 96. M. R. Gradoville, D. Bombar, B. C. Crump, R. M. Letelier, J. P. Zehr, A. E. White, Diversity and
58 activity of nitrogen-fixing communities across ocean basins. *Limnol Oceanogr* 2017, 62. 1895-1909,
59 DOI: 10.1002/lno.10542.
60

- 1
2
3 97. S. Kitajima, K. Furuya, F. Hashihama, S. Takeda, J. Kanda, Latitudinal distribution of
4 diazotrophs and their nitrogen fixation in the tropical and subtropical western North Pacific. *Limnol*
5 *Oceanogr* 2009, 54. 537-547.
6
7 98. M. Staal, S. T. Hekkert, G. J. Brummer, M. Veldhuis, C. Sikkens, S. Persijn, L. J. Stal, Nitrogen
8 fixation along a north-south transect in the eastern Atlantic Ocean. *Limnol Oceanogr* 2007, 52. 1305-
9 1316.
10
11 99. N. Gruber, in *Carbon-climate interactions*, ed. M. F. a. T. Oguz. John Wiley & Sons, 2004.
12
13 100. K. M. Orcutt, F. Lipschultz, K. Gundersen, R. Arimoto, A. F. Michaels, A. H. Knap, J. R. Gallon,
14 A seasonal study of the significance of N₂ fixation by *Trichodesmium* spp. at the Bermuda Atlantic Time-
15 series Study (BATS) site. *Deep-Sea Res Pt Ii* 2001, 48. 1583-1608.
16
17 101. W. Tang, N. Cassar, S. Wang, D. Fonseca P. Batista, F. Dehairs, S. Gifford, A. Gonzales, H.
18 Planquette, Coastal ocean broadens the biogeography of marine N₂ fixation. In prep.
19
20 102. D. G. Capone, J. P. Montoya, Nitrogen fixation and denitrification. *Methods in microbiology*
21 2001, 30. 501-515.
22
23 103. M. I. Scranton, P. C. Novelli, A. Michaels, S. G. Horrigan, E. J. Carpenter, Hydrogen-Production
24 and Nitrogen-Fixation by *Oscillatoria-Thiebautii* during Insitu Incubations. *Limnol Oceanogr* 1987, 32.
25 998-1006.
26
27 104. A. Mahadevan, A. Tagliabue, L. Bopp, A. Lenton, L. Memery, M. Levy, Impact of episodic
28 vertical fluxes on sea surface pCO₂. *Philos Trans A Math Phys Eng Sci* 2011, 369. 2009-25, DOI:
29 10.1098/rsta.2010.0340.
30
31 105. A. P. Martin, M. Levy, S. van Gennip, S. Pardo, M. Srokosz, J. Allen, S. C. Painter, R. Pidcock,
32 An observational assessment of the influence of mesoscale and submesoscale heterogeneity on ocean
33 biogeochemical reactions. *Global Biogeochem Cy* 2015, 29. 1421-1438, DOI: 10.1002/2015gb005129.
34
35 106. M. Levy, D. Iovino, L. Resplandy, P. Klein, G. Madec, A. M. Treguier, S. Masson, K. Takahashi,
36 Large-scale impacts of submesoscale dynamics on phytoplankton: Local and remote effects. *Ocean*
37 *Model* 2012, 43-44. 77-93, DOI: 10.1016/j.ocemod.2011.12.003.
38
39 107. M. Levy, A. P. Martin, The influence of mesoscale and submesoscale heterogeneity on ocean
40 biogeochemical reactions. *Global Biogeochem Cy* 2013, 27. 1139-1150, DOI: 10.1002/2012gb004518.
41
42 108. M. M. Omand, E. A. D'Asaro, C. M. Lee, M. J. Perry, N. Briggs, I. Cetinic, A. Mahadevan,
43 Eddy-driven subduction exports particulate organic carbon from the spring bloom. *Science* 2015, 348.
44 222-225, DOI: 10.1126/science.1260062.
45
46 109. B. F. Jonsson, J. E. Salisbury, Episodicity in phytoplankton dynamics in a coastal region.
47 *Geophys Res Lett* 2016, 43. 5821-5828, DOI: 10.1002/2016gl068683.
48
49
50
51
52
53
54
55
56
57
58
59
60

1
2
3
4
5
6
7
8
9
10
11
12
13
14
15
16
17
18
19
20
21
22
23
24
25
26
27
28
29
30
31
32
33
34
35
36
37
38
39
40
41
42
43
44
45
46
47
48
49
50
51
52
53
54
55
56
57
58
59
60

Table 1. Abbreviations and symbols used in the description of the FARACAS method. “-” means that the values depend on the specific conditions. $[C_2H_4]_{chamber}^*$ is equal to $[C_2H_4]_{total}$ when the incubation chamber is well mixed.

Acronym	Description	value	unit
$[C_2H_4]_{total}$	ethylene concentration of seawater at outlet of the incubation chamber	-	parts per billion (ppb)
$[C_2H_4]_{chamber}^*$	ethylene concentration of incubated seawater in the incubation chamber	-	ppb
b	ethylene background concentration in the mixture of acetylene-enriched seawater and natural seawater	-	ppb
$[C_2H_4]_{ARA}$	ethylene produced from acetylene reduction in the incubation chamber	-	ppb
$[C_2H_4]_{strip}$	ethylene concentration in gas measured by CRDS	-	ppb
τ	residence time of the incubation chamber	90	min
V	volume of the incubation chamber	9000	mL
Q_{sw}	volumetric seawater flow rate carried by the peristaltic pump	85±0.085	mL min ⁻¹
Q_{tracer}	volumetric acetylene-enriched seawater flow rate	15±0.015	mL min ⁻¹
Q_{total}	volumetric flow rate of seawater and acetylene-enriched seawater	100±0.086	mL min ⁻¹
Q_{strip}	volumetric flow rate of gas stripping	35±0.5	mL min ⁻¹
N_{fixAR}	acetylene reduction rates	-	ppb C ₂ H ₄ min ⁻¹
N_{fix}	N ₂ fixation rates	-	nmol N ₂ L ⁻¹ d ⁻¹ (ppb N ₂ min ⁻¹)
X	ethylene extraction efficiency factor	0 – 1 (this study 0.66±0.03)	unitless
V_{bc}	volume of bubble column contactor	~140	mL
V_l	volume of liquid in bubble column contactor	-	mL
V_{hs}	volume of headspace in bubble column contactor	-	mL
V_{bb}	volume of bubbles in bubble column contactor	-	mL
V_{lbb}	volume of mixture of liquid and bubbles in bubble column contactor	-	mL

k_L	liquid phase mass transfer coefficient	-	m min^{-1}
ε_g	gas holdup	-	unitless
a	contactor's effective specific gas-liquid interfacial area	-	$\text{m}^2 \text{m}^{-3}$
α	Ostwald solubility coefficient	-	unitless
d_s	sauter mean bubble diameter	-	μm
r_{H_2O}	water vapor volume mixing ratio	-	unitless

Table 2. Gas extraction efficiencies under various ratios of stripping gas to water flow rates. De-ionized water was used in these experiments.

Q_{sw} (mL/min)	Q_{strip} (mL/min)	$[C_2H_4]_{strip_1}$ (ppb)	$[C_2H_4]_{strip_2}$ (ppb)	Extraction efficiency (X) (%)
35	400	11	1.5	86
80	400	19.5	4	79
120	400	23.6	7.6	68

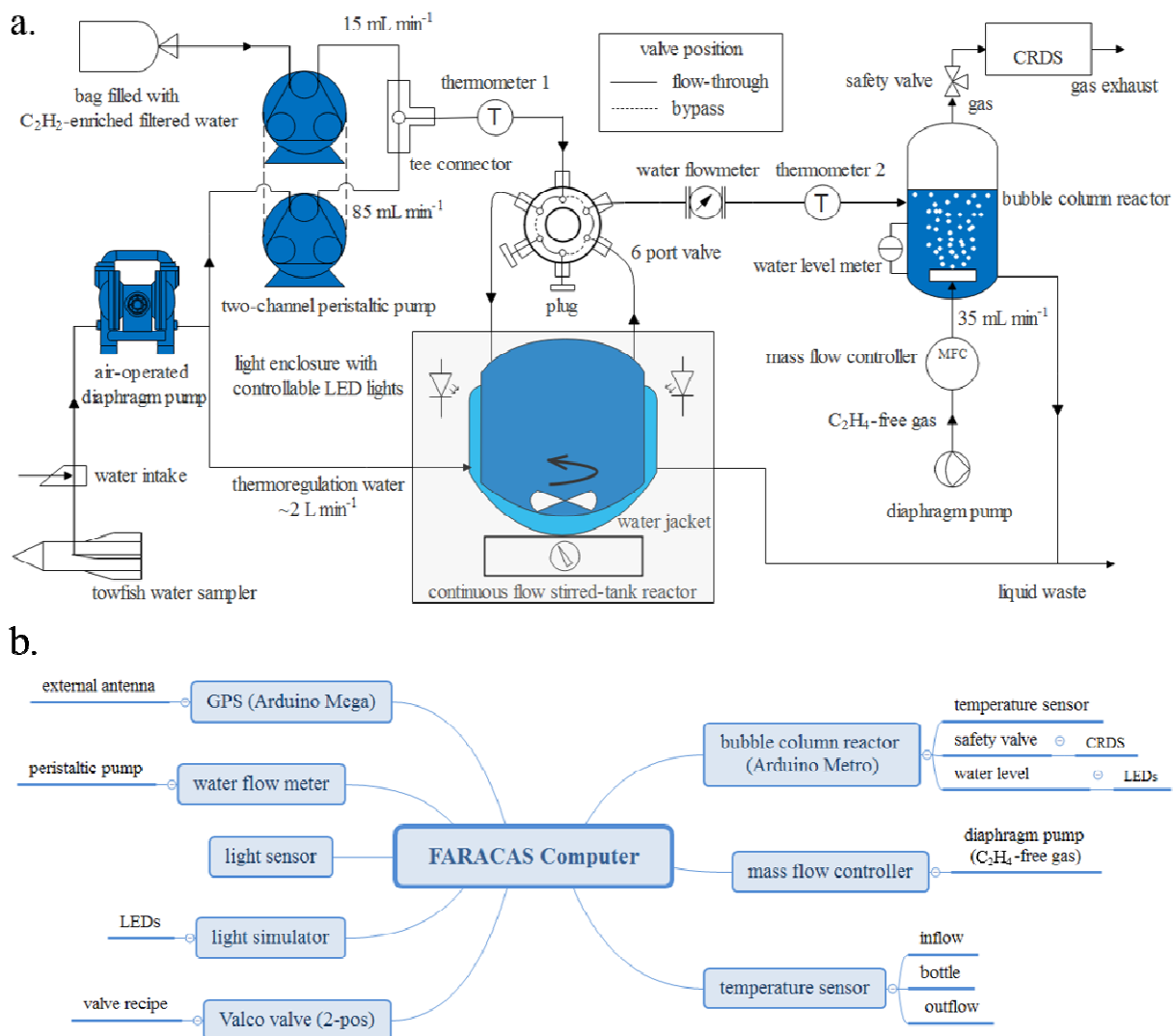


Figure 1: a. Schematic illustration of the FARACAS method for underway high-frequency N_2 fixation measurements. Seawater sampled with a towfish is continuously mixed using a dual-head peristaltic pump with a dissolved C_2H_2 solution prior to entering a flow-through incubation chamber, downstream of which the C_2H_4 is extracted with a bubble column contactor and allowed into the CRDS optical module. If the ambient air C_2H_4 concentration is too high or variable, an air cylinder can be used instead of the diaphragm pump for sparging in the bubble column contactor. b. Flow chart diagram of electrical components communicating with the computer in the FARACAS method.

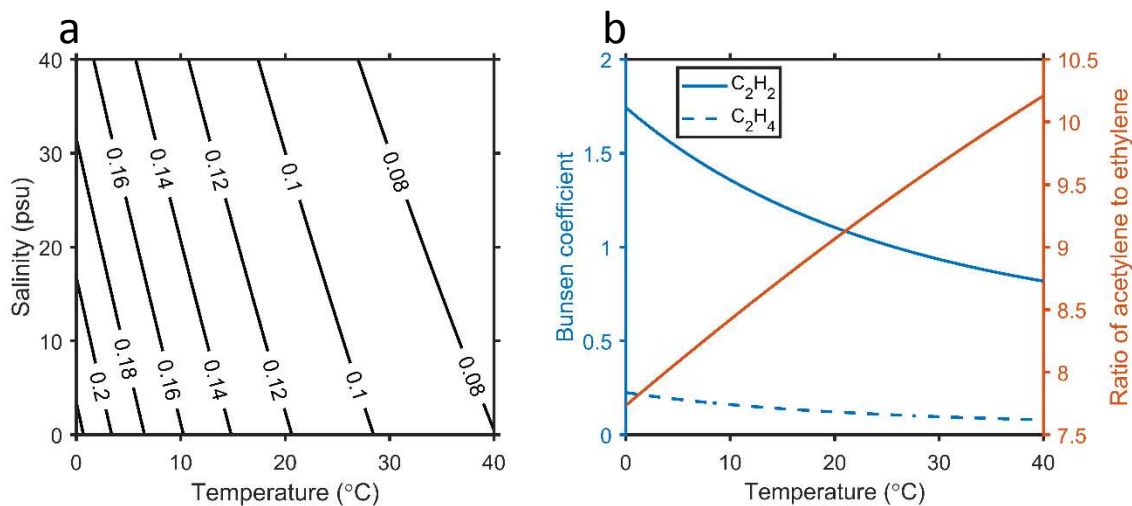


Figure 2: Ethylene (C_2H_4) and acetylene (C_2H_2) solubilities. a) Contour plot of C_2H_4 Bunsen solubility coefficient (unitless) as a function of temperature and salinity based on equations in ⁸⁸. b) C_2H_2 and C_2H_4 Bunsen solubility coefficients (unitless) and their ratio as a function of temperature at a salinity of zero.

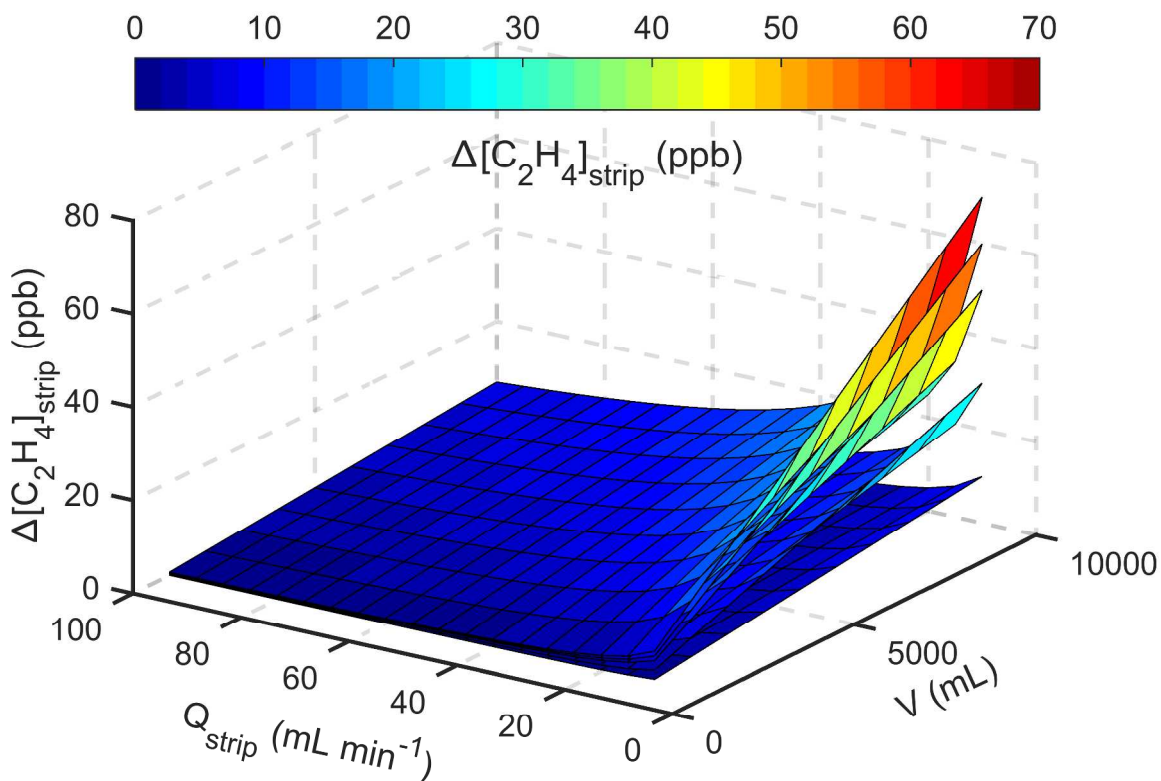


Figure 3: Modeled C_2H_4 difference between flow-through and bypass ($\Delta[C_2H_4]_{strip} = ([C_2H_4]_{strip} - [C_2H_4]_{strip_{\tau=0}})$) as a function of FARACAS incubation chamber volume and stripping gas flow rates for a C_2H_2 reduction rate of 0.1 ppb min^{-1} , a lower end of the range in tropical waters. From bottom to top, each surface represents an C_2H_4 extraction factor of 0.1, 0.3, 0.5, 0.6 and 0.7, respectively. Note that these calculations do not take into account the effect of the stripping gas sparging flow rate on the C_2H_4 gas extraction efficiency (X) (see Table 2 and discussion of empirical results).

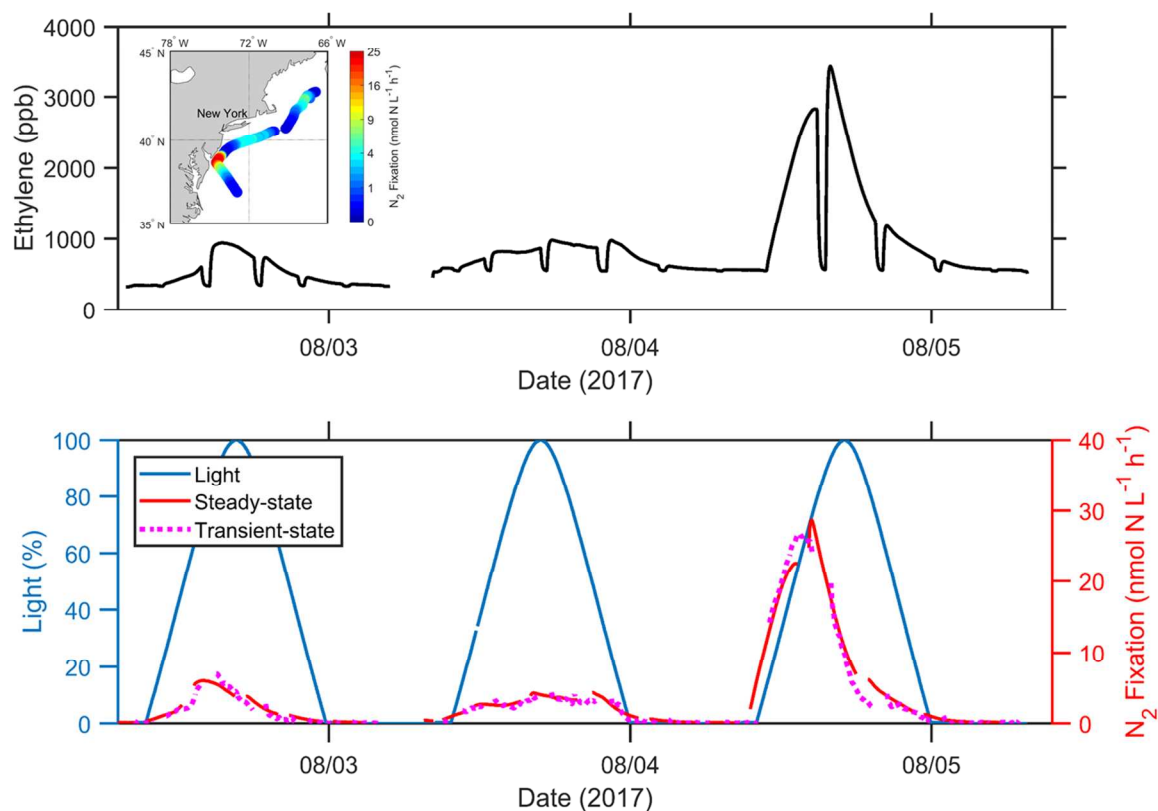
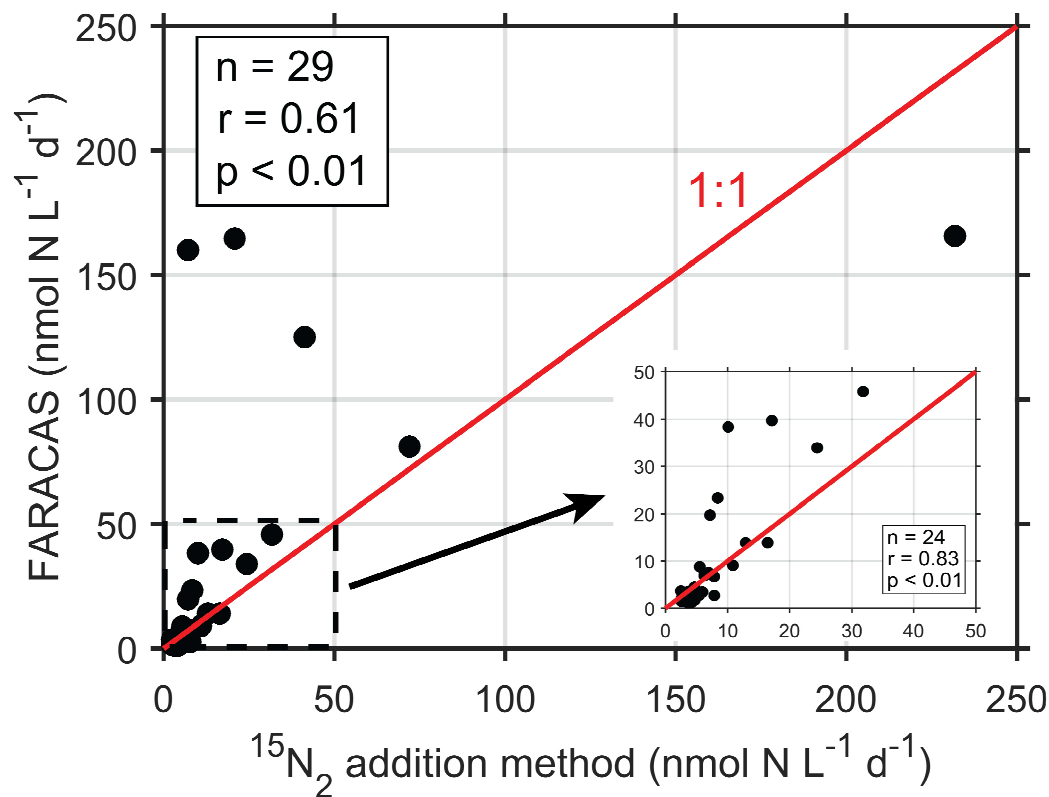


Figure 4. Example of FARACAS observations along the North American coast in the Atlantic Ocean. The upper panel represents the raw CRDS C_2H_4 signal with bypasses of the flow-through incubations every few hours. The second panel shows the calculated N_2 fixation rates using the raw data in the top panel with the steady-state (red) and transient-state (pink) equations. The

1
2
3 steady-state model is shifted 90-minute forward to account for the incubation time. Diel cycle in
4 diazotrophic activity can clearly be observed when compared to light intensity as shown on the
5 primary ordinate in blue.
6
7
8
9
10
11
12
13
14



41
42
43
44
45
46
47
48
49
50
51
52
53
54
55
56
57
58
59
60

Figure 5. Comparison with traditional ¹⁵N₂ addition method with zoomed-in inset with adjusted statistics. Identity (1:1) line represented with a red line. The daily underway N₂ fixation rates were calculated by integrating the FARACAS signal over 24 hours centered at the time when discrete samples were collected for the ¹⁵N₂ incubations. A C₂H₂/N₂ conversion of 4 is used to convert the acetylene reduction to N₂ fixation rates.